Atmospheric
Chemistry
and Physics

An experimental study of the reactivity of terpinolene and β-caryophyllene with the nitrate radical

Axel Fouqueau[1,2], Manuela Cirtog[1], Mathieu Cazaunau[1], Edouard Pangui[1], Jean-François Doussin[1], and Bénédicte Picquet-Varrault[1]

[1]LISA, Université Paris-Est Créteil and Université de Paris, CNRS, 94010 Créteil, France
[2]Department of Gas Metrology, Laboratoire National de Métrologie et d'Essais (LNE),
Paris CEDEX 15 75724, France

Correspondence: Bénédicte Picquet-Varrault (benedicte.picquet-varrault@lisa.ipsl.fr)

Abstract. Biogenic volatile organic compounds (BVOCs) are intensely emitted by forests and crops into the atmosphere. They can rapidly react with the nitrate radical (NO_3) during the nighttime to form a number of functionalized products. Among them, organic nitrates (ONs) have been shown to behave as reservoirs of reactive nitrogen and consequently influence the ozone budget and secondary organic aerosols (SOAs), which are known to have a direct and indirect effect on the radiative balance and thus on climate.

Nevertheless, $BVOC + NO_3$ reactions remain poorly understood. Thus, the primary purpose of this study is to furnish new kinetic and mechanistic data for one monoterpene ($C_{10}H_{16}$), terpinolene, and one sesquiterpene ($C_{15}H_{24}$), β-caryophyllene, using simulation chamber experiments. These two compounds have been chosen in order to complete the few experimental data existing in the literature. Rate constants have been measured using both relative and absolute methods. They have been measured to be $(6.0 \pm 3.8) \times 10^{-11}$ and $(1.8 \pm 1.4) \times 10^{-11}$ cm^3 molec.$^{-1}$ s^{-1} for terpinolene and β-caryophyllene respectively. Mechanistic studies have also been conducted in order to identify and quantify the main reaction products. Total organic nitrates and SOA yields have been determined. Both terpenes appear to be major ON precursors in both gas and particle phases with formation yields of 69 % for terpinolene and 79 % for β-caryophyllene respectively. They are also major SOA precursors, with maximum SOA yields of around 60 % for terpinolene and 90 % for β-caryophyllene. In order to support these observations, chemical analyses of the gas-phase products were performed at the molecular scale using a proton transfer reaction–time-of-flight–mass spectrometer (PTR-ToF-MS) and FTIR. Detected products allowed proposing chemical mechanisms and providing explanations through peroxy and alkoxy reaction pathways.

1 Introduction

Human and biologic activities emit a large number of trace compounds into the atmosphere, including volatile organic compounds (VOCs). At the global scale, 90 % of the VOCs are emitted by biogenic activities (Guenther et al., 1995). Biogenic VOCs (BVOCs) include isoprene (C_5H_8), monoterpenes ($C_{10}H_{16}$), sesquiterpenes ($C_{15}H_{24}$) and oxygenated compounds. Most of them are unsaturated VOCs and react rapidly with atmospheric oxidants, leading to lifetimes below a minute for the most reactive ones. The NO_3 radical has

been shown to be an efficient oxidant of these compounds not only during the nighttime but also during the daytime under low-sunlight conditions, e.g., below the forest canopy (Brown and Stutz, 2012).

These reactions lead to the formation of organic nitrates (ONs) which behave as reservoirs for reactive nitrogen by undergoing long-range transport in the free troposphere before decomposing and releasing NO_x in remote regions (Ng et al., 2017). They therefore significantly influence the reactive nitrogenous species (NO_y) and ozone budgets in these

regions (Ito et al., 2007). Multifunctional organic nitrates are also expected to partition into condensed phases (aerosols, droplets), and this was confirmed by field observations which have shown that organic nitrates range from 10 % to 75 % of total organic aerosol (OA) mass (Kiendler-Scharr et al., 2016; Lee et al., 2016; Xu et al., 2015). ONs are therefore important components of OAs. A good understanding of the reactions of BVOCs and NO$_3$ is thus necessary to better assess the impact of these processes on air quality and radiative forcing. Nevertheless, for a number of BVOCs, this chemistry remains poorly studied.

In this study, we have investigated the reactivity of the NO$_3$ radical with two BVOCs, terpinolene (a monoterpene) and β-caryophyllene (a sesquiterpene) (see Fig. 1), using simulation chambers for determining both rate constants and mechanisms, with an experimental protocol similar to the one used in Fouqueau et al. (2020a). Terpinolene represents 30 % of *Sassafras albidum* monoterpene emissions, and the global emission is estimated to be 1.3 Tg yr^{-1} (Guenther et al., 2012). β-Caryophyllene is considered to be the most emitted sesquiterpene. It is also among the most emitted BVOCs by pine trees: it is the fifth most emitted compound by *Pinus taeda* (3 % of total emissions, 47 identified species) and the second one by *Pinus virginiana* (10 % of total emissions, 34 identified species), with a global emission of 7.4 Tg yr^{-1}. Despite these two compounds having been detected in many tree emissions (Geron et al., 2000), their reactions with NO$_3$ radicals have been subject to a few studies only, and little is known about this reactivity. Terpinolene has been subject to one absolute rate determination (Martinez et al., 1999) and two relative studies (Corchnoy and Atkinson, 1990; Stewart et al., 2013). The relative value measured by Corchnoy and Atkinson (1990) is almost 50 % higher than the other determinations. For β-caryophyllene, only one relative rate determination was conducted. No mechanistic study has ever been published for terpinolene to our knowledge, whereas three studies have been published for β-caryophyllene: SOA yield was measured by Jaoui et al. (2013), and the chemical composition of the aerosol phase was analyzed. This study shows that β-caryophyllene + NO$_3$ is a major source of SOA, with production yields estimated to be 150 %. Products in the particle phase were measured by collecting SOA on filters and by performing derivatization followed by GC-MS analyses. Mass spectra observed for NO$_3$ oxidation were shown to be very different from those measured for other oxidants, but no clear identification of the products was proposed. In addition, this study suggests that these products contain fewer nitrogen species than SOA from other terpenes (e.g., isoprene–NO$_3$ system). Fry et al. (2014) have also studied the SOA production from β-caryophyllene + NO$_3$. They have provided SOA yield plots and the organic nitrate fraction in total aerosol mass. Nevertheless, the consumption of BVOCs was very fast in this study, and this could lead to an overestimation of SOA yields. For this reason also, some parameters, like
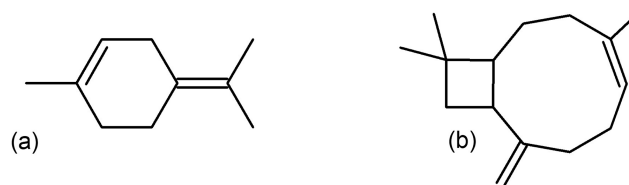
Figure 1. Molecular representation of terpinolene **(a)** and β-caryophyllene **(b)**.

ON yields, were not measured. Finally, Wu et al. (2021) studied the impact of photolysis on NO$_3$-generated SOA for β-caryophyllene. They measured a final SOA yield (110 %) and provided particle-phase composition analysis, showing a major impact of organic nitrates. Nevertheless, neither the Y_{SOA}-vs.-M_0 graph nor SOA model parameters were provided. In addition, β-caryophyllene concentrations could not be measured by the quadrupole proton transfer reaction–mass spectrometer (PTR-MS), due to its m/z ratio being outside the mass transmission range. New studies, both kinetic and mechanistic, are necessary to have a better understanding of the impact of these two compounds on air quality and radiative forcing.

2   Experimental section

The two different simulation chambers were used to study the reactions of terpinolene and β-caryophyllene with NO$_3$ radicals: the CSA chamber and the CESAM chamber. Absolute and relative rate determinations were conducted for both compounds. To tackle the determination of these very fast reactions, a highly sensitive technique was required for the monitoring of nitrate radicals. Absolute determinations were hence conducted using in situ incoherent broadband cavity-enhanced absorption spectroscopy (IBBCEAS), which was recently coupled with the CSA chamber (Fouqueau et al., 2020b). For both compounds, mechanistic studies have also been conducted in the CESAM chamber: total organic nitrate and SOA yields were determined, and several individual gas-phase products have been identified. Mechanisms have been proposed for the two compounds using this information.

2.1   Chamber facilities and analytical devices

Kinetic experiments were performed in the CSA chamber. It is a 6 m long – 977 L – Pyrex® reactor (Doussin et al., 1997) equipped with a homogenization system allowing a mixing time below 1 min (Fouqueau et al., 2020b). This chamber has been designed for the investigation of gas-phase chemistry and is thus equipped with instruments dedicated to gas-phase monitoring. For measuring organic and inorganic species in the chamber, an FTIR spectrometer (Bruker VERTEX 80) is coupled to an in situ multiple reflection optical system. Spec-

tra were recorded with a resolution of $0.5\,\mathrm{cm}^{-1}$, an optical path length of 204 m and a spectral range of $700\text{–}4000\,\mathrm{cm}^{-1}$.

During absolute kinetic experiments, an in situ IBBCEAS technique was used to monitor NO_3 radicals at the parts-per-trillion (ppt) level from its absorption at 662 nm. This technique is described in detail in Fouqueau et al. (2020b). It allows for the monitoring of NO_3 radicals at very low concentrations (parts-per-trillion level) and exhibits a very good time resolution (10 s). Simultaneously, it provides NO_2 concentration at the parts-per-billion (ppb) level. Before each experiment, the wavelength-dependent mirror reflectivity, $R(\lambda)$, has to be very precisely and accurately determined. For this purpose, a known amount of NO_2 of several hundreds of ppb was introduced into the chamber. To quantify both NO_3 and NO_2, cross sections were taken from Orphal et al. (2003) and Vandaele et al. (1997) respectively. At NO_3 maximum absorption (662.1 nm), the cross section is $(2.13 \pm 0.06) \times 10^{-17}\,\mathrm{cm}^2\,\mathrm{molec.}^{-1}$. Thanks to the very high reflectivity of the mirrors ($99.974\,\% \pm 0.002\,\%$), the maximum optical path length was calculated to be 2.5 km. This configuration leads to an NO_3 detection limit of 6 ppt for 10 s of integration time. The relative uncertainty in NO_3 concentration was estimated to be 9 %, with a minimum absolute value of 3 ppt (Fouqueau et al., 2020b).

To study the mechanisms and the SOA formation, experiments were carried out in the CESAM chamber (Experimental Multiphasic Atmospheric Simulation Chamber; Wang et al., 2011), which has been specifically designed to investigate multiphase processes. Briefly, it is a 4177 L stainless-steel evacuable reactor equipped with a fan that allows for efficient mixing within approximatively 1 min (Wang et al., 2011). Aerosol lifetimes in the CESAM chamber are up to 3 d (depending on particle size – see the Supplement in Lamkaddam et al., 2017), which makes it well suited for SOA studies. The chamber is equipped with dedicated analytical instruments for gas and aerosol phases. To monitor the gas-phase composition, an in situ long-path FTIR spectrometer (Bruker Tensor 37) is coupled to the chamber. It allows measuring spectra in the $700\text{–}4000\,\mathrm{cm}^{-1}$ spectral range with a resolution of $0.5\,\mathrm{cm}^{-1}$ and an optical path of 174.5 m. A proton transfer reaction–time-of-flight–mass spectrometer (PTR-ToF-MS) operating in both NO^+ and H_3O^+ ionization modes was also connected to the chamber. For the aerosol phase, a scanning mobility particle sizer (SMPS) composed of a TSI Classifier model 3080 and differential mobility analyzer (DMA) TSI model 3081 coupled to a condensation particle counter (CPC) TSI model 3772 allows the measurement of the particle size distribution between 20 and 880 nm. With the size distributions being measured in number, a particle density of $1.4\,\mathrm{g\,cm}^{-3}$ was used to convert them into mass distributions (Fry et al., 2014; Draper et al., 2015; Boyd et al., 2015).

Integrated band intensities (IBIs) used in this study to quantify species of interest using FTIR are (in $\mathrm{cm\,molec.}^{-1}$, logarithm base e) as follows:

- $IBI_{terpinolene}$ ($750\text{–}850\,\mathrm{cm}^{-1}$) $= (4.22 \pm 0.4) \times 10^{-19}$;

- $IBI_{\beta\text{-caryophyllene}}$ ($840\text{–}920\,\mathrm{cm}^{-1}$) $= (1.60 \pm 0.2) \times 10^{-18}$ (measured experimentally for this study);

- IBI_{NO_2} ($1530\text{–}1680\,\mathrm{cm}^{-1}$) $= (5.6 \pm 0.2) \times 10^{-17}$ (Rothman et al., 2003);

- IBI_{HNO_3} ($840\text{–}930\,\mathrm{cm}^{-1}$) $= (2.1 \pm 0.2) \times 10^{-17}$ (Hjorth et al., 1987);

- $IBI_{N_2O_5}$ ($1205\text{–}1275\,\mathrm{cm}^{-1}$) $= (1.7 \pm 0.1) \times 10^{-17}$ (Gordon et al., 2017).

This technique was also used to measure the total organic nitrate concentration, considering that all organic nitrates absorb at $850\,\mathrm{cm}^{-1}$ and that the intensity of this band is weakly affected by the chemical structure of the ON. In this study, IBI_{ON} ($900\text{–}820\,\mathrm{cm}^{-1}$) $= (9.5 \pm 2.9) \times 10^{-18}\,\mathrm{cm\,molec.}^{-1}$ was used (Fouqueau et al., 2020a).

In addition, a high-resolution PTR-ToF-MS (Kore Series 2e, mass resolution of 4000) was used, in both H_3O^+ and NO^+ ionization mode. With H_3O^+ ionization mode, i.e., the standard operational conditions, organic nitrates have been shown to be subject to important fragmentation (Müller et al., 2012; Aoki et al., 2007). To limit this, the electric field in the drift tube has been reduced following the protocol proposed by Duncianu et al. (2017). The instrument was also operated in NO^+ ionization mode by using dry air instead of water as ionization gas and by applying a reduced electric field in the reactor. In this mode, ONs are mainly ionized by charge transfer and by the formation of an adduct with NO^+ and hence are detected at their own mass M and at $M + 30$. Hydroxynitrates are a particular case, as they are detected at $M - 1$, suggesting an ionization process involving a hydrogen loss.
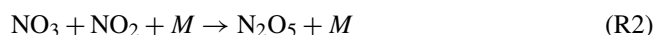
To measure total ON yield in the aerosol phase, filter sampling was performed during experiments. Following a protocol described by Rindelaub et al. (2015), filters were extracted in 5 mL of CCl_4 and then analyzed with FTIR. Using two standards of organic nitrates (nitrooxypropanol and *tert*-butyl nitrate), they were quantified with IBIs of 510 and $580\,\mathrm{L\,mol}^{-1}\,\mathrm{cm}^{-2}$ respectively between 1264 and $1310\,\mathrm{cm}^{-1}$. The integrated absorption cross section of organic nitrates in the liquid phase was found to be IBI_{ONs} ($1264\text{–}1310\,\mathrm{cm}^{-1}$) $= 557 \pm 110\,\mathrm{L\,mol}^{-1}\,\mathrm{cm}^{-2}$, the difference between the IBIs measured for the two compounds being smaller than the uncertainty.

Because instruments sampling causes a pressure decrease in the chamber, pure air is continuously injected to maintain constant pressure . The consequence is that the mixture is subject to progressive dilution. The dilution rate was calculated thanks to the measurement of the pure-air injection flow. For a typical flow rate of $1.7\,\mathrm{L\,min}^{-1}$, the gas mixture in the chamber is diluted by max 20 % after 3 h of experiment. All data presented here were corrected for dilution.

SOA measurements were also corrected for particle physical wall loss, which was parametrized as a function of the diameter of the particles and interpolated using the Lai and Nazaroff (2000) model (friction velocity $u^* = 3.7\,\mathrm{cm\,s^{-1}}$, from Lamkaddam et al., 2017). In the CESAM chamber, the wall loss appears to be very small (in comparison to Teflon chambers) thanks to stainless-steel walls that limit losses due to electrostatic effects.

2.2 Chemicals

Terpinolene and β-caryophyllene were purchased from Sigma-Aldrich at 95 % and 98 % purity respectively. Synthetic air to fill the chambers was generated using 80 % N_2 from liquid nitrogen evaporation (purity > 99.995 %, H_2O < 5 ppm, Messer) and 20 % O_2 (quality N5.0, purity > 99.995 %, H_2O < 5 ppm, Air Liquide). NO_3 radicals were generated in situ from using the thermal dissociation of N_2O_5 which was first synthesized in a vacuum line from a protocol adapted from Atkinson et al. (1984a) and Schott and Davidson (1958) and detailed in Picquet-Varrault et al. (2009). The synthesis proceeds in two steps: first NO_3 is formed by the reaction between O_3 and NO_2 (Reaction 1) and then reacts with NO_2 to form N_2O_5 (Reaction 2). After a purification stage by pumping the bulb containing N_2O_5 for a few minutes, it is introduced into the chamber and decomposes to form NO_3 radicals (Reaction 3).

$$O_3 + NO_2 \rightarrow NO_3 + O_2 \tag{R1}$$
$$NO_3 + NO_2 + M \rightarrow N_2O_5 + M \tag{R2}$$
$$N_2O_5 + M \leftrightharpoons NO_3 + NO_2 + M \tag{R3}$$

2.3 Kinetic study

Kinetic experiments were conducted in the CSA chamber at room temperature and atmospheric pressure, in a mixture of N_2/O_2 (80/20). Both relative and absolute rate methods were used for an accurate determination of the rate constants. For absolute rate determination, a PTR-ToF-MS and IBBCEAS were used to monitor BVOC and NO_3 concentrations respectively. Experiments were conducted by first introducing several hundred ppb of NO_2 into the chamber in order to determine the reflectivity of the IBBCEAS mirrors. Then, the BVOC was injected and left in the dark for approximatively 1 h. This allows checking for eventual wall loss or reaction with NO_2. No significant loss was observed. In order to limit SOA formation, which would strongly reduce the IBBCEAS signal due to light absorption and/or scattering and mirror soiling by particles, low BVOC mixing ratios have been used (between 15 and 90 ppb). In addition, the mirrors were flushed with nitrogen to protect them from particle deposition. Finally, NO_3 was generated in situ (see Sect. 2.1) by stepwise injections of N_2O_5, and measurements were performed with a time resolution of 10 s in order to allow mon-

itoring fast decay of reactants. Several stepwise injections of N_2O_5 were made until the complete BVOC consumption.

Considering the following reaction,

$$BVOC + NO_3 \rightarrow \text{products}, \tag{R4}$$

the second-order kinetic equation is obtained:

$$-\frac{d\,[BVOC]}{dt} = k_{BVOC}[BVOC][NO_3]. \tag{1}$$

For small time intervals, such as the time resolution used in this study, it can be approximated as

$$-\Delta[BVOC] = k_{BVOC}[BVOC][NO_3]\Delta t, \tag{2}$$

where $-\Delta[BVOC]$ is the decay of the BVOC during the Δt time interval and $[BVOC]$ and $[NO_3]$ are averaged concentrations during this interval. k_{BVOC} is obtained by plotting $-\Delta[BVOC]$ vs. $[BVOC] \times [NO_3] \times \Delta t$. It should be mentioned that the determination of the rate constant is thus not affected by losses of NO_3 due to reaction with other species (products, RO_2 radicals, etc.) as the rate constant is not deduced from the NO_3 consumption rate but from the BVOC one. The uncertainty in k_{BVOC} was taken as twice the standard deviation of the slope.

For relative rate determination, PTR-ToF-MS and FTIR techniques were used to monitor the BVOC decay relatively to a reference compound. As with absolute rate experiments, the organic reactants were left in the dark for 1 h prior to the N_2O_5 injection. By assuming that consumption by NO_3 is the only fate of the studied BVOC and the reference compound and that these compounds are not a product of both of the reactions, the following equation can be shown (Atkinson, 1986):

$$ln\left(\frac{[BVOC]_{t_0}}{[BVOC]_t}\right) = \frac{k_{BVOC}}{k_{Ref.}} ln\left(\frac{[Ref.]_{t_0}}{[Ref.]_t}\right), \tag{3}$$

where $[BVOC]_{t_0}$ and $[Ref.]_{t_0}$ are BVOC and reference concentrations at time t_0 (which correspond to the moment before the beginning of the oxidation), $[BVOC]_t$ and $[Ref.]_t$ are the concentrations at t time, and k_{BVOC} and $k_{Ref.}$ are the rate constants with NO_3.

In this work, 2,3-dimethyl-2-butene was used as reference compound because of its well-known rate constant with NO_3 radicals. In absence of a recommendation by IUPAC, the value recommended by Calvert et al. (2015) and by McGillen et al. (2020) was used. However, the uncertainty proposed by these recommendations is very high (150 %) despite the fact that experimental determinations are in good agreement. So, uncertainty was reevaluated and calculated as the mean value of the determinations available in the literature (Berndt et al., 1998; Benter et al., 1992; Lancar et al., 1991; Rahman et al., 1988; Atkinson et al., 1988, 1984a, b). The obtained value is $k_{\text{2,3-dimethyl-2-butene}} = (5.7 \pm 1.7) \times 10^{-11}\,\mathrm{cm^3\,molec.^{-1}\,s^{-1}}$. The same value and corresponding uncertainty were used

by Newland et al. (2022). Finally, the uncertainty in k_{BVOC} was calculated by considering the relative uncertainty corresponding to the statistical error in the linear regression (2σ) and the error in the reference rate constant.

2.4 Mechanistic study

A mechanistic study was conducted in the CESAM chamber at room temperature and atmospheric pressure, in a mixture of N_2/O_2 (80/20). Experiments were typically conducted by first introducing the BVOC into the chamber and leaving it in the dark for approximatively 1 h to estimate possible wall and/or dark losses. No significant wall loss was observed for both studied BVOCs ($k_d < 10^{-7} \, \text{s}^{-1}$). Then N_2O_5 was introduced by slow continuous injections as this method has been observed to be more efficient than stepwise injections in slowing down the oxidation and thus better controlling the SOA formation. A PTR-ToF-MS and FTIR spectrometer were used to monitor both BVOC and gas-phase products. In some experiments, two PTR-ToF-MSs were used in order to detect gas-phase products in both NO^+ and H_3O^+ ionization modes simultaneously. If using two instruments was not possible, experiments were duplicated. An SMPS was used to monitor the SOA production. Because of the lack of standards, quantification of gas-phase products measured by the PTR-ToF-MS was not possible. In order to measure SOA yields under low aerosol content, no seed particles were introduced into the chamber. Filter sampling was performed for experiments for which the concentration of the precursor was up to 150 ppb. It started when the precursor had completely reacted and lasted for 3 to 6 h. To avoid the condensation of gas-phase products on the filter, a charcoal denuder was used.

When products could be quantified by FTIR, their formation yields were calculated by plotting their molecular concentration against the reacted BVOC molecular concentration and by calculating the slope at the origin. To calculate the total organic nitrate yields in the SOA phase, the final organic nitrate concentration measured on the filters was divided by the total reacted BVOC concentration. Uncertainties in formation yields were calculated as the sum of the relative uncertainties in the product and the BVOC cross sections and twice the standard deviation of the linear regression. Organic nitrates have been measured in both gas and particle phases. Consequently, a total organic nitrate yield has been calculated, being the addition of these two yields. Their uncertainties were calculated as the sum of the relative uncertainties in gas- and particle-phase yields.

SOA yield is defined as the ratio between the produced SOA mass concentration, M_0, and the reacted BVOC mass concentration, ΔBVOC. It was calculated for each data point and after the total consumption of the BVOC for all experiments, providing time-dependent and overall SOA yields. Uncertainties in SOA yields were calculated as the sum of the relative errors in VOC concentrations measured by FTIR and the SOA concentration measured by the SMPS. Know-

ing both the organic nitrate yield in the particle phase and the total SOA yield, the ratio $Y_{\text{ONp, mass}} / Y_{\text{SOA, mass}}$ has been calculated. Uncertainties were calculated as the sum of relative errors in Y_{ONp} and Y_{SOA}.

SOA yields were plotted against the organic aerosol mass, and a fit was applied using a two-product model described by Odum et al. (1996):

$$Y = M_0 \left[\frac{\alpha_1 K_{\text{p},1}}{1 + K_{\text{p},1} M_0} + \frac{\alpha_2 K_{\text{p},2}}{1 + K_{\text{p},2} M_0} \right], \tag{4}$$

where α_1 and α_2 and $K_{\text{p},1}$ and $K_{\text{p},2}$ are stoichiometric factors and partitioning coefficients (in $\text{m}^3 \, \mu\text{g}^{-1}$) of the two hypothetical products respectively. It was expected that SOA equilibrium would be reached in small time steps because of the slow injections of N_2O_5; thus time-dependent yields have been used. Hence, yields for small aerosol content have also been obtained.

In order to assess their contribution to SOA formation, vapor pressures P^{vap} have been evaluated using the SIMPOL.1 method (Pankow and Asher, 2008) via the GECKO-A website (http://geckoa.lisa.u-pec.fr, last access: 5 March 2021). In order to estimate the fraction of a product i in the condensed phase ξ^i_{aer}, Raoult's law has been used (Valorso et al., 2011):

$$\xi^i_{\text{aer}} = \frac{N_{i,\text{aer}}}{N_{i,\text{aer}} + N_{i,\text{gas}}} = \frac{1}{1 + \frac{\overline{M_{\text{aer}}} \gamma_i P_i^{\text{vap}}}{C_{\text{aer}RT}} \times 10^6}, \tag{5}$$

where $N_{i,\text{gas}}$ and $N_{i,\text{aer}}$ are respectively the gas- and particle-phase concentrations (in molecules cm^{-3}) of the product i, $\overline{M_{\text{aer}}}$ the SOA species mean molecular weight ($\text{g} \, \text{mol}^{-1}$), C_{aer} is the total SOA mass concentration ($\mu\text{g} \, \text{m}^{-3}$), R the gas constant ($\text{atm} \, \text{m}^3 \, \text{K}^{-1} \, \text{mol}^{-1}$), T the temperature (K), P_i^{vap} the vapor pressure and γ_i the product i activity coefficient ($\gamma_i = 1$ was used in this study). Here, $\overline{M_{\text{aer}}}$ has been estimated to be the mean molecular weight of detected low-volatility products.

The calculation of ξ^i_{aer} depends strongly on the estimation of P^{vap}. It was shown by Pankow and Asher (2008) that SIMPOL.1 technique predicts it with an uncertainty between 50 % and 60 % for $P^{\text{vap}} < 10^{-6}$ atm. The uncertainty can reach 80 % for $P^{\text{vap}} = 10^{-10}$ atm. ξ^i_{aer} can only be used as a guide, because it is associated with a high uncertainty. ξ^i_{aer} has also be compared to the partitioning coefficients K_{p} used in Eq. (4):

$$K_{\text{p}} = \frac{N_{i,\text{aer}}}{N_{i,\text{gas}}} \times \frac{1}{C_{\text{aer}}} = \frac{\xi^i_{\text{aer}}}{1 - \xi^i_{\text{aer}}} \times \frac{1}{C_{\text{aer}}} \tag{6}$$

3 Kinetic results

All experiments and their conditions are presented in Table 1. Both of the compounds were subject to absolute and relative rate determinations. For each method, between two and four experiments were conducted.

Table 1. Experimental conditions of kinetic experiments. $[BVOC]_i$ and $[Ref.]_i$ are the initial mixing ratios of the BVOC and of the reference compound. For $[N_2O_5]$, the number of punctual injections is indicated in parentheses. T is the mean temperature inside the simulation chamber during the experiment.

BVOC	Date (yyyy/mm/dd)	Method*	$[BVOC]_i$ (ppb)	Ref.	$[Ref.]_i$ (ppb)	$[N_2O_5]_i$ (ppb)	$[NO_2]_i$ (ppb)	T (K)
Terpinolene	2018/04/25	RR	190	2,3-dimethyl-2-butene	210	200 (2 inj.), 300	–	295.15
	2018/04/26		540	2,3-dimethyl-2-butene	420	100, 200 (2 inj.), 300	–	294.55
			240	2,3-dimethyl-2-butene	330	300 (3 inj.), 400	–	294.85
	2018/04/24	AR	15	–	–	20 (2 inj.)	750	295.45
			31	–	–	40 (2 inj.)	740	295.55
	2018/04/25		45	–	–	40 (2 inj.)	890	295.15
β-Caryophyllene	2018/04/20	RR	550	2,3-dimethyl-2-butene	360	200, 300 (2 inj.), 600	–	295.45
			690	2,3-dimethyl-2-butene	650	200, 400 (2 inj.), 600	–	295.45
	2018/04/18	AR	45	–	–	20 (3 inj.)	540	294.85
			86	–	–	20 (3 inj.)	560	295.05
	2018/04/19		67	–	–	20 (2 inj.)	560	295.35
			36	–	–	20 (2 inj.)	590	295.55

* RR: relative rate determination; AR: absolute rate determination.

Kinetic results obtained by the relative rate method are plotted in Fig. 2. They present good linear tendencies and are in good agreement whatever the analytical technique used. For both individual data sets obtained by a PTR-ToF-MS and FTIR, linear regressions have been first performed separately. The results being in good agreement, a global linear regression was applied to all the data, leading to $k_{terpinolene} = (6.0 \pm 2.5) \times 10^{-11}$ cm^3 molec.$^{-1}$ s^{-1} and $k_{\beta\text{-caryophyllene}} = (1.4 \pm 0.7) \times 10^{-11}$ cm^3 molec.$^{-1}$ s^{-1}.

Absolute kinetic plots are shown in Fig. 3. Experimental points are rather scattered, and this can be explained by the low integration time used for PTR-ToF-MS and IBBCEAS measurements. As a consequence, rate constants are subject to relatively high uncertainties. Rate constants measured by the absolute rate method are $(4.9 \pm 1.4) \times 10^{-11}$ cm^3 molec.$^{-1}$ s^{-1} for terpinolene and $(2.0 \pm 0.6) \times 10^{-11}$ cm^3 molec.$^{-1}$ s^{-1} for β-caryophyllene.

The values measured by both the relative and the absolute methods are compared to those already published in the literature in Table 2. In order to compare our values with literature data, the relative rate from Corchnoy and Atkinson (1990) has been recalculated using the same value for the reference rate constant (see Sect. 2.3). The value obtained by Stewart et al. (2013) with limonene as the reference compound was also recalculated using the latest IUPAC recommendation: $(1.2 \pm 0.4) \times 10^{-11}$ cm^3 molec.$^{-1}$ s^{-1}. Finally, the rate constant provided by Shu and Atkinson (1995) was recalculated using the value $(9.6 \pm 1.6) \times 10^{-11}$ cm^3 molec.$^{-1}$ s^{-1} for 2-methyl-2-butene. This value has been obtained by averaging all determinations published in the literature. The total uncertainties presented in this table for relative rate determinations

are the sum of the statistical errors provided by the authors and the errors in the reference rate constants.

For terpinolene, the absolute and relative determinations obtained in this work are in good agreement. They also appear to be in good agreement with the values provided by previous studies, within uncertainties. Nevertheless, when considering the k_{COVB}/k_{ref} values obtained in this work and by Corchnoy and Atkinson (1990) (both were using the same reference compound), it appears that the two relative rate determinations are not in agreement. The value obtained by Corchnoy and Atkinson (1990) is 40 % higher than that in our study. No explanation has been found for this difference, but it can be seen that the value of Corchnoy and Atkinson (1990) is higher than every other value in the literature. Our result thus confirms the lower values found by previous studies. For β-caryophyllene, the absolute and relative determinations obtained in this work are also in good agreement. These determinations have been compared to the only determination previously published by Shu and Atkinson (1995). A good agreement can be observed, whatever the method used. Our study provides the first absolute rate determination for β-caryophyllene. Our data were also compared to estimated rate constants using the structure–activity relationship (SAR) developed by Kerdouci et al. (2014). Experimental and estimated rate constants show a good agreement.

The terpinolene rate constant can be compared to the values found by Fouqueau et al. (2020a) for α-terpinene and γ-terpinene and is shown in Table 2. They indeed have very similar structures, only differing by the position of the double bonds. α-Terpinene and γ-terpinene have endocyclic double bonds (conjugated and not conjugated respectively), whereas terpinolene has one endocyclic and one exocyclic double
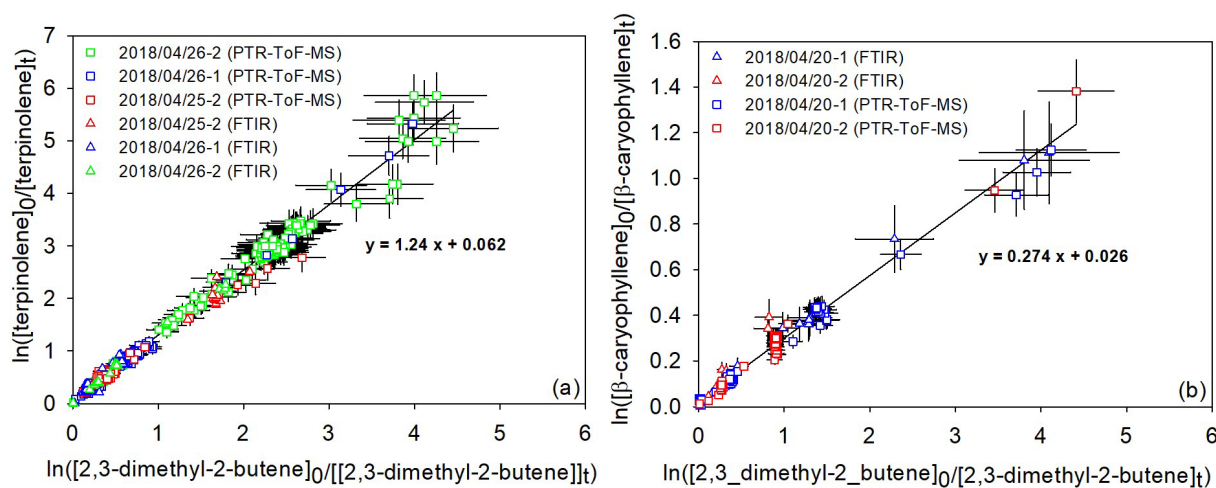
Figure 2. Relative kinetic plots measured by FTIR (triangle marks) and a PTR-ToF-MS (square marks) for terpinolene **(a)** and β-caryophyllene **(b)**.
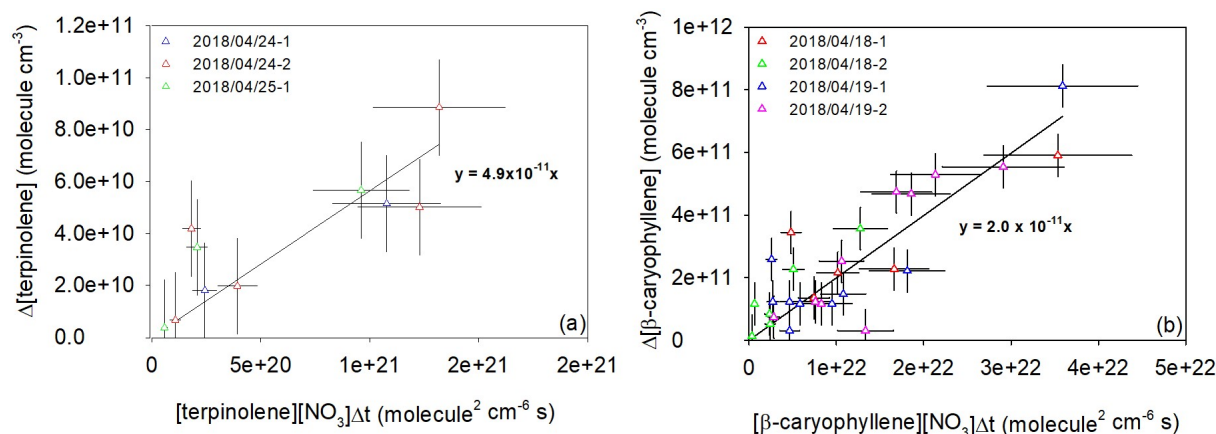
Figure 3. Absolute kinetic plots for terpinolene **(a)** and β-caryophyllene **(b)**.

bond. α-Terpinene appears to be much more reactive than γ-terpinene due to the conjugation of double bonds which leads to a stabilization of the transition state by resonance. Here, terpinolene is almost twice more reactive than γ-terpinene, and this can be explained by the substitution of the exocyclic double bond which stabilizes the adduct. In addition, terpinolene, which has non-conjugated C=C bonds, is less reactive than α-terpinene.

4 Mechanistic results

Seven mechanistic experiments were conducted in the CE-SAM chamber for terpinolene and nine for β-caryophyllene. During experiments, the formation of gas-phase products and SOA was monitored. Table 3 presents experimental conditions together with organic nitrates and SOA yields that were measured. As an example, reactant and product time profiles (corrected for dilution) are presented in Fig. 4 for the ex-

periment on 18 December 2017 on terpinolene. In the first minutes following N_2O_5 injection (marked by the red area), a competition occurs between the reactivity of NO_3 on the BVOC and its wall loss through N_2O_5 hydrolysis. In the beginning of the experiment, mainly nitric acid is thus formed by N_2O_5 hydrolysis on lines and chamber walls. Then, the BVOC starts to be oxidized with the weakening of the hydrolysis reaction. Because small quantities of N_2O_5 were introduced continuously in order to ensure a progressive oxidation of the BVOC, N_2O_5 concentration remains below the detection limit as long as the BVOC is not totally consumed (around 25 min here). The formation of large amounts of organic nitrates and SOA is observed: for an initial terpinolene mixing ratio of 180 ppb, up to 70 ppb of total organic nitrates and 400 $\mu g\,m^{-3}$ of aerosol are formed. Figure 4 also shows the aerosol size distribution. It can be seen that particles have mean diameters around 300–400 nm. PTR-ToF-MS

Table 2. Rate constants for the NO_3-initiated oxidation of terpinolene and β-caryophyllene: results from this study and comparison with the literature. Rate constants of α- and γ-terpinene found by Fouqueau et al. (2020a) are also shown. The results of our study are in bold.

BVOC	k (cm^3 molec.$^{-1}$ s^{-1})	$(k_{\mathrm{COVB}}/k_{\mathrm{ref}})$	Study (method)
Terpinolene	$\mathbf{(4.9 \pm 1.4) \times 10^{-11}}$		**This study (AR[a])**
	$\mathbf{(7.0 \pm 2.5) \times 10^{-11}}$	$\mathbf{(1.2 \pm 0.1)}$	**This study (RR[b]: 2,3-dimethyl-2-butene)**
	$(8.5 \pm 3.4) \times 10^{-11}$	(1.7 ± 0.1)	Corchnoy and Atkinson (1990) (RR[b]: 2,3-dimethyl-2-butene)
	$(5.2 \pm 0.9) \times 10^{-11}$		Martinez et al. (1999) (AR[a])
	$(6.2 \pm 3.0) \times 10^{-11}$		Stewart et al. (2013) (RR[b]: limonene)
	6.6×10^{-11}	(5.1 ± 0.4)	Estimated with SAR (Kerdouci et al., 2014)
β-Caryophyllene	$\mathbf{(2.0 \pm 0.6) \times 10^{-11}}$		**This study (AR[a])**
	$\mathbf{(1.5 \pm 0.7) \times 10^{-11}}$	$\mathbf{(0.27 \pm 0.04)}$	**This study (RR[b]: 2,3-dimethyl-2-butene)**
	$(2.0 \pm 0.7) \times 10^{-11}$	(2.1 ± 0.4)	Shu and Atkinson (1995) (RR[b]: 2-methyl-2-butene)
	2.1×10^{-11}		Estimated with SAR (Kerdouci et al., 2014)
γ-Terpinene	$(2.9 \pm 1.1) \times 10^{-11}$		Fouqueau et al. (2020a)
α-Terpinene	$(1.2 \pm 0.3) \times 10^{-10}$		Fouqueau et al. (2020a)

[a] Absolute rate determination. [b] Relative rate determination.

signal (m/z) time profiles are presented in Fig. S1 in the Supplement and are discussed later with their identification.

For β-caryophyllene, only two experiments could be used to determine the SOA yields. Indeed, except for experiments conducted in December 2017, very large amounts of SOA were formed (between 500 µg m^{-3} and 1 mg m^{-3}), and the upper part of the size distribution fell out of the SMPS range, affecting the relevance of the mass evaluation from SMPS measurement.

4.1   SOA yields

Figure 5 shows time-dependent and overall SOA yields (Y_{SOA}) as a function of the aerosol mass (M_0) for both terpinolene and β-caryophyllene. As explained before (see Sect. 2.4), a two-product model defined by Odum et al. (1996) has been applied for the two compounds. Final yields obtained for terpinolene can reach 60 %, whereas they are between 50 % and 90 % for β-caryophyllene. These results demonstrate both of the compounds are very efficient SOA precursors.

For terpinolene, our study provides the first determination of SOA yields. Figure 5 shows that fitted plots are well constrained for small aerosol contents (below 50 µg m^{-3}) thanks to the high number of experimental points in this area. This is a consequence of the slow injection of N_2O_5, which allows progressive BVOC oxidation. Fitted parameters have been found to be $\alpha_1 = 0.6$ and $K_{\mathrm{p},1} = 6.7 \times 10^{-3}$ m^3 µg^{-1} and $\alpha_2 = 3 \times 10^{-3}$; $K_{\mathrm{p},2} = 3.5 \times 10^{-1}$ m^3 µg^{-1}. The very low stoichiometric factor α_2 indicates that the second class of products is negligible, so the particle-phase products can be simulated with only one family of the same volatility. One can estimate the uncertainties in fitting parameters by looking at the fit sensitivity. It appears to be very sensitive to α
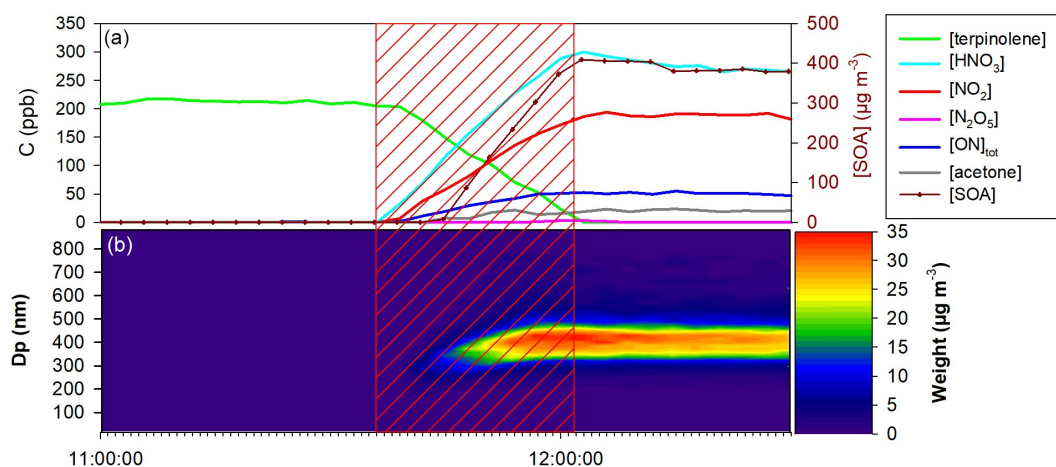
(with an associated error estimated to be 5 %) and less so to K_{p} (with an error estimated to be 50 %). For an aerosol mass concentration typical of a biogenic SOA-affected environment of 10 µg m^{-3} (Slade et al., 2017), an SOA yield of 5 % has been measured for terpinolene. For higher aerosol mass loading, which can be observed in polluted atmospheres (between 500 and 1000 µg m^{-3}), yield reaches 50 %–60 %.

For β-caryophyllene, a high dispersion is observed between the data from the two experiments, for low aerosol mass loadings that correspond to the first stages of the oxidation. For the experiment on 22 December 2017, an "unusual" profile is observed in the sense that the SOA yield decreases with the increasing M_0. This suggests that, despite a slow injection of N_2O_5, the oxidation of the β-caryophyllene was too fast in comparison to the mixing time, leading to a locally high concentration of semi-volatile species and, therefore, to an overestimation of the SOA yield. After a few minutes, the SOA yield decreases and is then in good agreement with those measured for the experiment on 15 December 2017, suggesting that semi-volatile species are better mixed in the reactor and therefore SOA yields are more accurate. The Odum fitting parameters obtained from these two experiments are $\alpha_1 = 0.5$ and $K_{\mathrm{p},1} = 4.1 \times 10^{-1}$ m^3 µg^{-1} and $\alpha_2 = 3.8 \times 10^{-3}$ and $K_{\mathrm{p},2} = 5 \times 10^{-1}$ m^3 µg^{-1}. As with terpinolene, the high value of α_1 and low α_2 indicate that one class of products, having a high partitioning coefficient ($K_{\mathrm{p},1}$), contributes mainly to the SOA formation. These results also show that β-caryophyllene is a very efficient SOA precursor with a yield close to 40 % at 10 µg m^{-3}, which can reach almost 60 % for higher aerosol mass loading. Nevertheless, due to the experimental problems mentioned above, this model is not well constrained for low aerosol mass loading (<100 µg m^{-3}), and these results have to be taken with

Table 3. Experimental conditions, ONs and SOA yields for mechanistic experiments conducted in the CESAM chamber. The use of an instrument is shown by an "x" and the non-use by a dash.

BVOC	Date (yyyy/mm/dd)	$[BVOC]_i$ (ppb)*	N_2O_5 injection (concentration and/or duration)	PTR-ToF-MS (NO^+)	PTR-ToF-MS (H_3O^+)	Filter sampling & analysis	$Y_{acetone}$, molar	Y_{ONg}, molar	Y_{ONp}, molar	$Y_{ON(g+p)}$, molar	Y_{ONp}, mass	Y_{SOA} mass	$Y_{ONp,mass}$ / $Y_{SOA,mass}$
Terpinolene	2017/04/03	300	Continuous (30 min)	x	–	x	0.31 ± 0.03	0.54 ± 0.07	0.23 ± 0.08	0.77 ± 0.37	0.36 ± 0.14	0.64 ± 0.17	0.56 ± 0.37
	2017/04/21	350	Continuous (35 min)	x	–	x	0.25 ± 0.03	0.52 ± 0.04	0.17 ± 0.07	0.69 ± 0.34	0.31 ± 0.12	0.47 ± 0.17	0.66 ± 0.49
	2017/04/24	360	Continuous (55 min)	–	x	x	0.18 ± 0.02	0.41 ± 0.04	0.19 ± 0.07	0.60 ± 0.28	0.27 ± 0.10	0.63 ± 0.18	0.42 ± 0.28
	2017/12/12	48	Continuous (17 min)	x	x	–	0.21 ± 0.02	0.21 ± 0.01	–	–	–	0.25 ± 0.09	–
		120	Continuous (48 min)	x	x	–	0.18 ± 0.02	0.25 ± 0.04	–	–	–	0.29 ± 0.09	–
	2017/12/13	120	Continuous (23 min)	x	x	–	0.11 ± 0.03	0.25 ± 0.02	–	–	–	0.33 ± 0.09	–
	2017/12/18	180	Continuous (24 min)	x	x	x	0.11 ± 0.03	0.30 ± 0.01	0.07 ± 0.03	0.37 ± 0.17	0.11 ± 0.04	0.41 ± 0.11	0.27 ± 0.17
β-Caryophyllene	2016/12/14	490	Continuous (11 min)	x	x	–	–	0.68 ± 0.03	–	–	–	exceeded range	–
		390	Continuous (56 min)	x	x	–	–	0.50 ± 0.01	–	–	–	exceeded range	–
	2016/12/15	530	Continuous (60 min)	x	–	–	–	0.48 ± 0.01	–	–	–	exceeded range	–
		450	Continuous (45 min)	x	–	–	–	0.49 ± 0.01	–	–	–	exceeded range	–
	2016/12/16	410	Continuous (12 min)	x	–	–	–	0.57 ± 0.02	–	–	–	exceeded range	–
	2017/04/04	840	Continuous (48 min)	x	–	x	–	0.57 ± 0.03	0.21 ± 0.09	0.78 ± 0.37	0.31 ± 0.12	exceeded range	–
	2017/04/28	430	Continuous (37 min)	–	x	x	–	0.53 ± 0.01	0.24 ± 0.09	0.77 ± 0.30	0.35 ± 0.13	exceeded range	–
	2017/12/15	80	Continuous (20 min)	x	x	x	–	0.52 ± 0.09	–	–	–	0.51 ± 0.14	–
	2017/12/22	230	Continuous (49 min)	x	x	x	–	0.41 ± 0.01	0.25 ± 0.09	0.66 ± 0.25	0.34 ± 0.13	0.43 ± 0.11	0.79 ± 0.50

* For all experiments, the BVOC was totally consumed.

Figure 4. Dilution-corrected time-dependent concentration of gaseous species, aerosol mass, SOA size distribution during a typical experiment of NO_3-initiated oxidation of terpinolene (18 December 2017). The hatched red area corresponds to the N_2O_5 injection period. **(a)** Terpinolene, N_2O_5, NO_2, HNO_3, acetone and total ONs from FTIR and SOA mass concentration from the SMPS; **(b)** SOA size distribution in mass concentration from the SMPS. The time zone of the time scale is UTC+1.
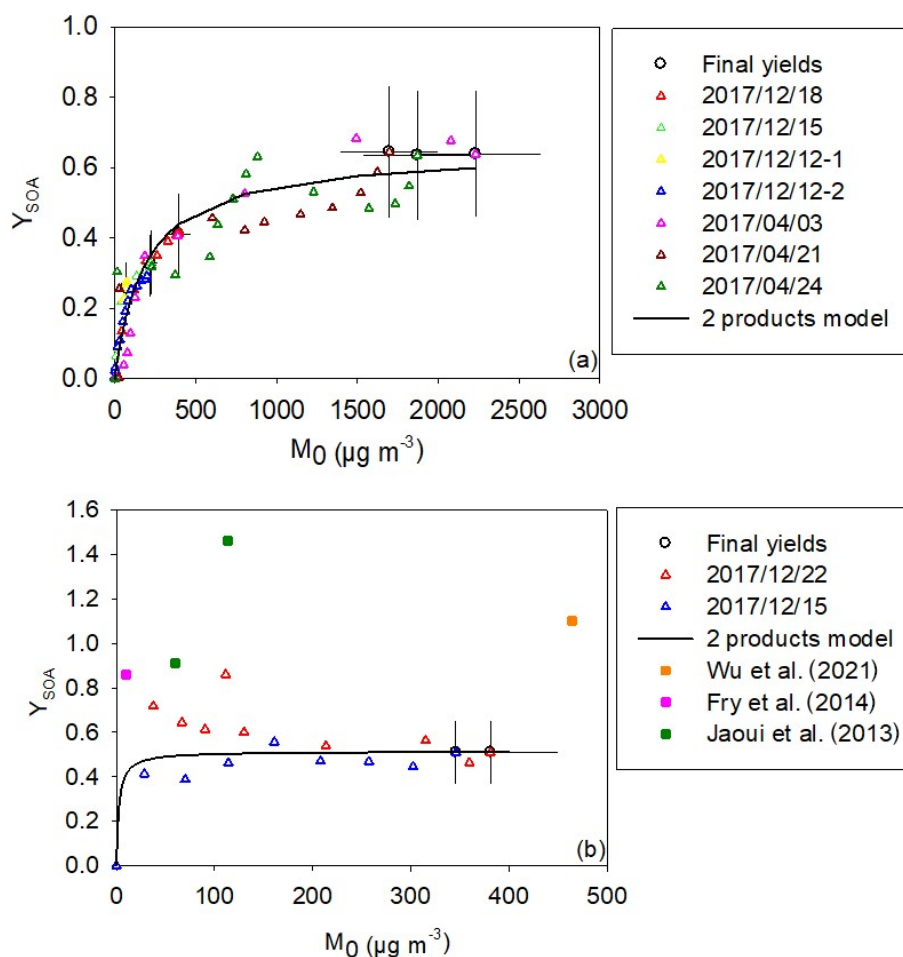
Figure 5. SOA yield as a function of the organic aerosol mass concentration measured for terpinolene **(a)** and for β-caryophyllene **(b)**. Final yields (circle marks) are shown with uncertainties. Data were fitted with a two-product model (black curve). For β-caryophyllene, literature values are presented by squared marks.

caution. Three studies have been previously conducted on the SOA production from β-caryophyllene. First, Jaoui et al. (2013) measured SOA yields in a simulation chamber. In this study, final aerosol yield has been provided without indication of the aerosol mass loading, thus preventing fitting data by the Odum model. Yields were shown to range between 91 % and 146 %. The Fry et al. (2014) study has provided SOA yields curves and ON yields in the particle phase. This study has been conducted with high and low BVOC concentrations (3 and 109 ppb respectively). Since experiments were carried out by introducing the oxidant into the chamber prior to the BVOC, the latter began to react immediately, preventing measurement of its initial concentration. The consumption of the BVOC had therefore to be estimated. In a similar way to our study, the authors have observed differences between high- and low-concentration mass yield curves, suggesting that the experiments differ in more than simply the total aerosol mass loading. They measured higher yields for high-concentration experiments than for low-concentration experiments (for the same aerosol mass loading). The authors recommend preferentially using data obtained for low-concentration experiments considering that due to the slower reaction, the ΔVOC is better constrained for longer periods and the mixing timescale is faster relative to reactions, resulting in more precise yield curves. However, even for these low-concentration experiments, the yields obtained (around 80 %) are much higher than those measured in our study. Such disagreement could be explained by the fact that ΔVOC is not precisely measured in the Fry et al. (2014) study. Another possible explanation provided by the authors that could explain the difference between high- and low-concentration experiments and also the disagreement between their results and our study may lie in the differences in the RO_2 radical fate. RO_2 radicals can indeed react following several pathways, in particular with NO_3 or with other RO_2 radicals, and products resulting from these two reactions differ. For example, $RO_2 + RO_2$ reactions can produce hydroxynitrates, which have low volatility and can thus participate to SOA formation (see discussion in Sect. 4.3). Finally, Wu et al. (2021) studied the photolytically induced aging of NO_3-initiated SOA. In order to fulfill this aim, they first generated SOA by reacting β-caryophyllene and NO_3. One experiment was conducted with 50 ppb of precursor, and a final SOA yield of 110 % was calculated. Two issues are pointed out: firstly, they could not monitor β-caryophyllene with a quadrupole PTR-MS because its m/z ratio was out of the range for quantitative measurement. The method used to calculate its concentration is then not explained, but it is probably associated with a larger uncertainty. Secondly, a concentration of more than 200 ppb of N_2O_5 is injected during approx. 10 s. As explained before, this can lead to an SOA yield overestimation and thus explain the observed differences. Nevertheless, the mean diameter of the size distribution measured in the study is between 229 and 266 nm, which is in good agreement with the ones mea-

sured here (between 225 and 246 nm at the end of the oxidation). The Wu et al. (2021) study showed no evaporation of SOA during dark aging, which agrees with the fact that SOA concentrations are stable here, after the oxidation. In conclusion, this discussion illustrates well how SOA yields may be affected by a number of parameters and how comparisons are difficult to interpret.

4.2 Organic nitrate yields

The total ON yields have been measured in the gas phase (Y_{ONg}). Their concentrations have been plotted against the consumption of the BVOC for both of the studied compounds in Fig. 6. The plots show a good linearity, and the slope at the origin is different from zero. This indicates that (i) organic nitrates are primary products and (ii) if they themselves react with NO_3 by addition to the other C=C bond, they produce secondary organic nitrates, so the total ON yield is constant during the course of the experiments as FTIR measurement cannot differentiate primary and secondary organic nitrates. Previous studies performed in the CESAM chamber have reported that ONs may be subject to wall losses, through absorption on the stainless-steel walls (Suarez-Bertoa et al., 2012; Picquet-Varrault et al., 2020). Loss rates have been found to be between 0.5 and $2 \times 10^{-5}\,\mathrm{s}^{-1}$. In this study, because ON yields were calculated for a short period (max 1 h), wall losses at this timescale are estimated to be less than 10 %. This is confirmed by the good linearity of the plots.

Molar Y_{ONg} values were found to be 47 % $\pm$ 10 % for terpinolene and 43 % $\pm$ 10 % for β-caryophyllene. These yields are in good agreement with previous studies performed for other BVOCs and show that ONs are major products of BVOC + NO_3 reactions. ON yields measured for isoprene and monoterpenes are indeed higher than 30 %. For example, limonene ON yields vary between 30 % and 72 % (Fry et al., 2014; Hallquist et al., 1999; Spittler et al., 2006) and β-pinene between 40 % and 74 % (Fry et al., 2014; Hallquist et al., 1999; Boyd et al., 2015). For α- and γ-terpinene (Fouqueau et al., 2020a) very close yields (47 % and 44 % respectively) have been measured. The only exception is α-pinene, for which yields vary between 10 % and 30 % (Fry et al., 2014; Hallquist et al., 1999; Spittler et al., 2006). Its main product is indeed an aldehyde, with a high vapor pressure, that does not contribute to the SOA phase.

Organic nitrates may partition between gas and aerosol phases. Hence, yields of total organic nitrates in the particle phase (Y_{ONp}) have been determined using FTIR analyses of the collected filters. Results are shown in Table 3. For terpinolene, molar yields range between 7 % and 23 %. The variability in these yields can be explained by the fact that, as SOA yields, they depend on the reacted BVOC concentration. They are thus probably overestimated in comparison with real atmospheric conditions. Indeed, for high-concentration experiments ($\sim$ 350 ppb), yields are around 20 %, whereas they are around 7 % for the low-concentration
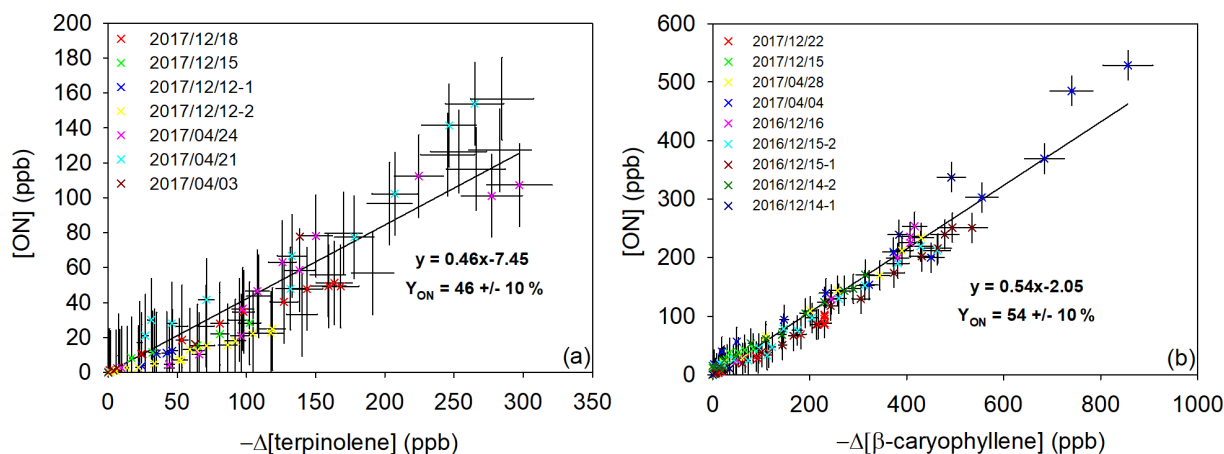
Figure 6. Gas-phase organic nitrate production vs. loss of terpinolene **(a)** and of β-caryophyllene **(b)**.

experiments (~ 180 ppb). For β-caryophyllene, Y_{ONp} values range between 21 % and 25 % and appear to be less subject to variability.

In order to evaluate the fraction of organic nitrates in SOA, Y_{ONp} values have been compared to SOA yields. For this comparison, both yields have to be expressed in mass. To do so, a unique molecular weight which is representative of the expected oxidation products has been considered: for terpinolene, a hydroxynitrate ($C_{10}H_{17}O_4N$) having a molecular weight of 215 g mol^{-1} has been chosen. For β-caryophyllene, the same type of compound has been chosen ($C_{15}H_{25}NO_3$), with a molecular weight of 283 g mol^{-1}. Both compounds were detected as oxidation products by PTR-ToF-MS. It is clear that this assumption generates a large error in ON mass yield, particularly if other products are formed with higher molecular weights (e.g., by polymerization in condensed phase). Nevertheless, as oxidation products were not quantified individually, this method is the only way to estimate the contribution of ONs to the aerosol phase. The ratio $Y_{ONp, mass}/YS_{OA, mass}$ values are also shown in Table 3. From these results, it is estimated that organic nitrates represent ~ 50 % of the SOA for terpinolene and ~ 80 % for β-caryophyllene and are therefore major components of the SOA produced by BVOC + NO$_3$ reaction. It should be noted that if higher-molecular-weight products were formed, these ratios would be even greater. The value obtained for β-caryophyllene is in very good agreement with the ratio of 80 % provided by Fry et al. (2014). These results are also in good agreement with field studies (Kiendler-Scharr et al., 2016; Ng et al., 2017) which have observed that organic nitrates are major components of organic aerosols, with a proportion that can reach almost 80 %. Even if organic nitrates can be produced by other reactions, an enhancement of organic nitrates in SOA has been observed by several studies in regions impacted by the NO$_3$ radical during the night (Gómez-González et al., 2008; Hao et al., 2014; Iinuma et al., 2007) and also in forest regions affected by urban air masses
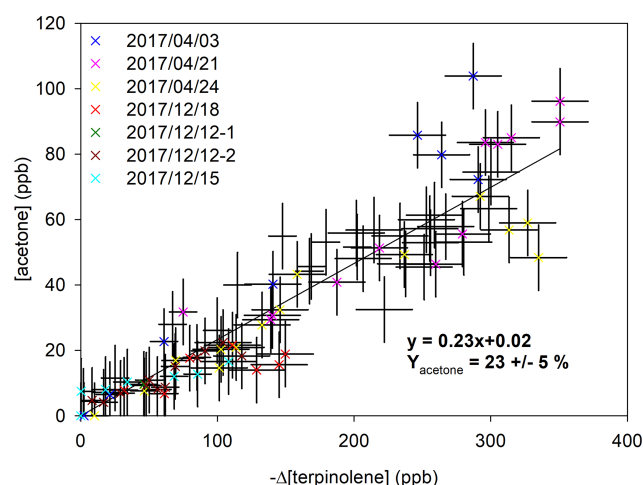
Figure 7. Acetone production vs. loss of terpinolene.

(Hao et al., 2014). This result thus confirms the major contribution of organic nitrates in SOA formation.

4.3 Products at molecular scale and mechanisms

To propose explanations for the measured yields, mechanisms have been built, using the molecular-scale PTR-ToF-MS identification of gas-phase products. By using two ionization modes (i.e., H$_3$O$^+$ and NO$^+$), a double identification of the molecules was possible. Detected signals in both ionization modes and corresponding raw formulae are summarized in Table 4. Products with molecular weights of 58, 142 and 168 g mol^{-1} for terpinolene have been detected with high intensities. For β-caryophyllene, the main signals were measured for products having molecular weights of 221 and 236 g mol^{-1}. In Table 4, intensities are shown following this logic: the one or two most intense peak are marked "+ + +" and are usually at least 1 order of magnitude higher than the other ones. Peaks that are more intense than 10 counts are

marked "++", and the other ones are marked "+". Many of the products which were detected are nitrogenous species, which is in good agreement with the measurement of high organic nitrate yields. Mechanisms have been proposed in Fig. 8 for terpinolene and in Fig. 9 for β-caryophyllene. Time profiles of PTR-ToF-MS signals (see Fig. S1 in the Supplement) were also used to determine whether the products are primary or secondary ones. First-generation products are framed in blue and second-generation ones in red.

In addition, for experiments on terpinolene, acetone was detected by FTIR and its formation yield has been measured. Figure 7 shows the concentration of acetone plotted against the consumption of terpinolene. Every experiments shows similar and linear tendencies, within uncertainties. Acetone appears to be a primary product, with a production yield of $23\% \pm 5\%$. Terpinolene is thus a major precursor of acetone.

4.3.1 Terpinolene oxidation scheme

The NO_3 radical reacts with terpinolene by addition onto one of the two double bonds (H-atom abstraction is considered negligible), each addition leading to the formation of two possible nitrooxy-alkyl radicals. According to the SAR developed by Kerdouci et al. (2014), the exocyclic double bond is expected to be 5 times more reactive than the endocyclic one as it is more substituted. Nevertheless, all possible pathways were considered here, but the pathways for only two radicals are presented in Fig. 8 in order to facilitate the reading (see Fig. S2 for the two others). In most cases, the products formed are isomers and cannot be distinguished from one path to another with the techniques used here.

Nitrooxy-alkyl radicals can then react with O_2 to form a peroxy radical (RO_2) via reaction 2 in Fig. 8. The formation of an epoxide has also been observed ($152\,g\,mol^{-1}$, reaction 3 in Fig. 8), using both NO^+ (m/z 152) and H_3O^+ (m/z 153) ionization modes. RO_2 radicals then react following different pathways: they can react with NO_2 to form a peroxynitrate, RO_2NO_2 ($MW = 276\,g\,mol^{-1}$, where MW denotes molecular weight), following reaction 4 in Fig. 8. This was detected in NO^+ ionization mode at m/z 276. This reaction is usually negligible in the atmosphere but can be significant in simulation chambers due to high NO_2 concentrations. It should also be noted that peroxynitrates (RO_2NO_2), which have a characteristic absorption in the IR region, were not detected in our experiments, neither in the gaseous phase nor in the aerosol one. This suggests that $RO_2 + NO_2$ reactions are minor pathways. It can also react with another peroxy radical ($RO_2 + RO_2$, reaction 5 in Fig. 8) to form a characteristic hydroxynitrate ($MW = 215\,g\,mol^{-1}$) and a ketonitrate ($MW = 213\,g\,mol^{-1}$). Both were detected at m/z 216 ($M + 1$) in H_3O^+ ionization mode and m/z 214 ($M - 1$) in NO^+ mode for the hydroxynitrate and at m/z 214 ($M + 1$) in H_3O^+ mode and 243 ($M + 30$) in NO^+ mode for the ketonitrate. This reaction involving an H-atom transfer is possible only if the carbon that carries the peroxy radical group is linked to a hydrogen, i.e., for primary and secondary peroxy radicals. Here, this reaction is thus possible only for the peroxy radical coming from the addition on the endocyclic double bond shown in Fig. 8. Finally, peroxy radicals can react with another RO_2 or with the NO_3 radical (reactions 6 and 6' respectively in Fig. 8) to form an alkoxy radical (RO).

RO radicals can then evolve following reactions 7, 8 and 9 in Fig. 8. They can react with O_2 (reaction 7) to form the same ketonitrate as the one formed by reaction 5 ($MW = 213\,g\,mol^{-1}$). In the case of NO_3 addition onto the endocyclic double bond, the resulting alkoxy radical can decompose following reaction 8, leading to the formation of an alkyl radical, which then reacts following previously mentioned pathways to form a diketonitrate ($MW = 229\,g\,mol^{-1}$, framed in green in Fig. 8). This trifunctional product has been detected in both H_3O^+ (m/z 230) and NO^+ ionization modes (m/z 229). This alkoxy radical can also decompose by a scission of the $C(ONO_2)$–$CH(O^\bullet)$ bond (reaction 9), leading to the formation of a dicarbonyl ring opening product of $MW = 168\,g\,mol^{-1}$ (detected at m/z 169 in H_3O^+ mode and m/z 168 in NO^+ mode). In the case of NO_3 addition onto the exocyclic double bond, the resulting alkoxy can decompose to form a carbonyl product of $MW = 110\,g\,mol^{-1}$ (detected at m/z 111 in H_3O^+ mode and m/z 110 in NO^+ mode) and acetone. Acetone has been detected with a formation yield of 23%. Considering that this pathway is the only one allowing the primary production of acetone, a tentative determination of the branching ratio has been made. As mentioned previously, NO_3 addition to the exocyclic double bond is expected to be the major pathway. The two resulting alkoxy radicals (see Fig. S3) can both produce acetone by decomposition but with different expected yields. The radical shown in Fig. 8, i.e., the one having the radical group on the isopropyl group, is expected to produce mainly acetone, whereas the other one shown in Fig. S2, i.e., the one having the radical group on the cycle, is expected to decompose following the three possible pathways, which have very close activation energies (Vereecken and Peeters, 2009). Thus, considering the same probability for the three decomposition pathways, acetone production yield would be around 30%. Experimental acetone yield being 23%, this would suggest that the alkoxy having the radical group on the cycle is predominant.

Primary products can themselves react with NO_3 because they still possess a double bond, leading to the formation of second-generation products, squared in red in Fig. 8. Second-generation products coming from the carbonyl and the dicarbonyl products have been identified: a tricarbonyl compound ($MW = 142\,g\,mol^{-1}$) and two epoxides ($MW = 184\,g\,mol^{-1}$ and $MW = 126\,g\,mol^{-1}$).

Calculated vapor pressures and their estimated partition in the SOA are shown next to the products in Fig. 8. Among the first-generation products, two are likely to participate in SOA formation: the hydroxynitrate and the diketonitrate. The hydroxynitrate is a product characteristic of the $RO_2 + RO_2$ pathway and has a low vapor pressure because of the pres-
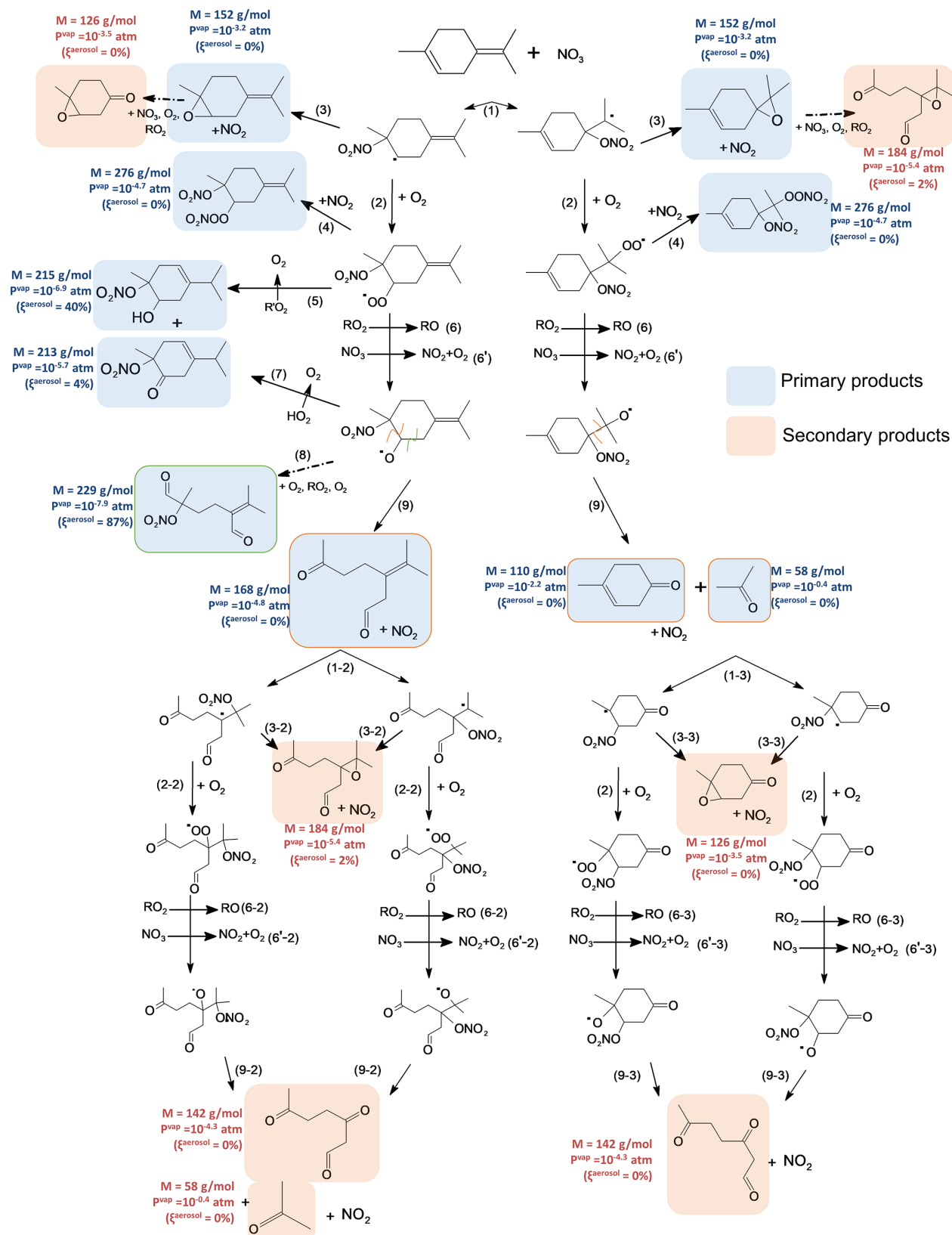
Figure 8. Proposed mechanism for terpinolene. First-generation products are squared in blue and second-generation ones in red. Alkoxy fragmentation products are squared according to the location of the fragmentation. Molecular weight, vapor pressures and the gas–particle partition are shown next to the molecules.
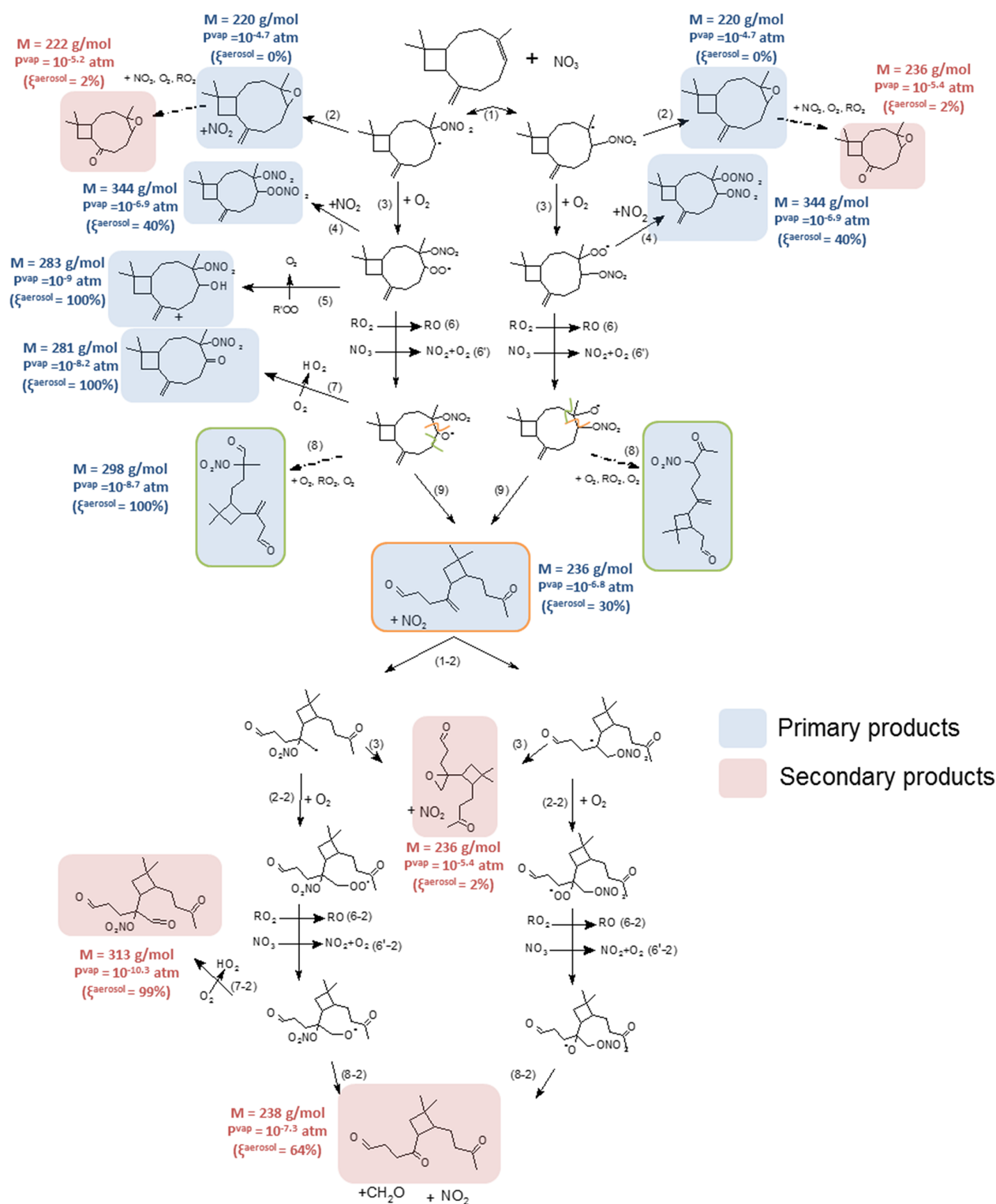
Figure 9. Proposed mechanism for β-caryophyllene. First-generation products are squared in blue and second-generation ones in red. Alkoxy fragmentation products are squared according to the location of the fragmentation. Molecular weight, vapor pressures and the gas–particle partition are shown next to the molecules.

Table 4. Products detected for terpinolene (a) and β-caryophyllene (b) with PTR-ToF-MS H_3O^+ and NO^+ ionization modes: formulae and molar masses, detected masses, ionization processes (H^+: proton adduct; NO^+: NO^+ adduct; CT: charge transfer; PL: proton loss), peak intensity, and comportment.

| | Molecule | | H_3O^+ ionization mode | | | | NO^+ ionization mode | | | |
	Raw formula	M (g mol^{-1})	m/z	Process	Intensity	Behavior	m/z	Process	Intensity	Behavior
(a)	C_3H_6O	58	59.0579	H^+	+++	Primary	58.0411	CT	++	Primary
	$C_7H_{10}O$	110	111.0842	H^+	++	Primary	110.0753	CT	++	Primary
	$C_7H_{10}O_{22}$	126	127.0642	H^+	++	Primary	126.0584	CT	+	Primary
	$C_7H_{10}O_3$	142	143.0581	H^+	++	Primary	142.0539	CT	+++	Primary
	$C_{10}H_{16}O$	152	153.1171	H^+	++	Secondary	/	/	/	/
	$C_{10}H_{16}O_2$	168	169.0952	H^+	+	Primary	168.1038	CT	+++	Primary
	$C_{10}H_{16}O_3$	184	185.0877	H^+	++	Primary	/	/	/	/
	$C_8H_{17}N_2O_4$	205	/	/	/	/	205.17	CT	+	Secondary
	$C_{10}H_{15}NO_4$	213	214.1262	H^+	+	Primary	/	/	/	/
	$C_{10}H_{17}NO_4$	215	216.0816	H^+	+	Primary	214.1174	PL	+	Primary
							245.1796	NO^+	+	Primary
	$C_{10}H_{15}NO_5$	229	230.0836	H^+	++	Primary	229.1056	CT	+	Primary
	$C_9H_{15}NO_6$	233	234.0635	H^+	+	Detected	233.0877	CT	+	Primary
	$C_{10}H_{15}NO_6$	245	246.0999	H^+	+	Primary	/	/	/	/
	$C_{10}H_{15}NO_7$	261	262.1143	H^+	+	Detected	/	/	/	/
	$C_{10}H_{16}N_2O_7$	276	/	/	/	/	276.1304	CT	+	Detected
	$C_8H_{18}N_2O_9$	286	287.1717	H^+	+	Detected	/	/	/	/
	$C_{10}H_{14}O_{10}$	294	295.0404	H^+	+	Detected	293.0629	PL	+	Detected
(b)	$C_{15}H_{24}O$	220	221.1674	H^+	+++	Primary	220.2033	CT	++	Primary
	$C_{14}H_{22}O_2$	222	223.1717	H^+	+	Secondary	222.1779	CT	+	Secondary
	$C_{15}H_{24}O_2$	236	237.2017	H^+	+++	Primary	236.202	CT	+++	Primary
	$C_{14}H_{22}O_3$	238	239.2183	H^+	+	Secondary	/	/	/	/
	$C_{15}H_{24}O_3$	252	253.1838	H^+	+	Secondary	252.2279	CT	+	Detected
	$C_{14}H_{22}NO_4$	267	268.2034	H^+	+	Detected	267.3576	CT	+	Detected
	$C_{15}H_{23}NO_3$	281	282.1562	H^+	++	Primary	311.2733	NO^+	+	Detected
	$C_{15}H_{25}NO_3$	283	284.2149	H^+	+	Primary	282.4786	PL	++	Primary
	$C_{15}H_{25}NO_5$	298	299.1841	H^+	+	Primary	298.2353	CT	+	Primary
	$C_{15}H_{23}NO_6$	313	314.2904	H^+	+	Detected	/	/	/	/
	$C_{15}H_{23}N_2O_6$	327	/	/	/	/	327.1502	CT	+	Detected
	$C_{15}H_{24}N_2O_7$	344	345.2471	H^+	+	Detected	/	/	/	/

ence of hydrogen bonds. This compound is estimated to be at 40 % in the SOA phase. However, considering that the addition of NO_3 proceeds mainly by addition onto the exocyclic double bond, the formation of the hydroxynitrate is expected to be minor. The diketonitrate (MW $= 229$ g mol^{-1}) is also expected to significantly contribute to SOA formation with a partition of 90 % in the SOA phase. It can be formed by additions of NO_3 onto both the exocyclic and the endocyclic C=C bonds. For this trifunctional product, the associate partitioning coefficient, K_p, has been calculated following Eq. (6). Considering the uncertainty in ξ_{aer}^i due to the vapor pressure estimation, it can vary from 1.1×10^{-2} to 3.4×10^{-3} m^3 µg^{-1}. This value is consistent with the partitioning coefficient found with the two-product model from Eq. (4) ($K_{p,1} = 6.7 \times 10^{-3}$ m^3 µg^{-1}), within the associated estimated uncertainty in K_p.

Identified secondary products have high vapor pressures and thus may not contribute to the SOA formation. Other products with molecular weights close to 290 g mol^{-1} have been detected with weak signals but were not identified. Due to their high molecular weights, they could significantly contribute to SOA. In addition, other secondary products may be

formed without being detected by PTR-ToF-MS due to their too low volatility.

4.3.2 β-Caryophyllene oxidation scheme

β-Caryophyllene has two double bonds, one exocyclic and one endocyclic, but according to the Kerdouci et al. (2014) SAR, the exocyclic bond is expected to be approx. 40 times less reactive than the endocyclic one CH=C < because it is less substituted. So only the addition onto the endocyclic bond has been considered here, leading to the formation of two possible nitrooxy-alkyl radicals (see Fig. 9).

Like for terpinolene, alkyl radicals can evolve following two pathways: (i) the formation of an epoxide (MW $= 220$ g mol^{-1}, reaction 2 in Fig. 9), detected at m/z 221 in H_3O^+ ionization mode and m/z 220 in NO^+ mode, and (ii) the formation of a peroxy radical, by reaction with O_2 (reaction 3 in Fig. 9). Under high NO_2 levels, RO_2 radicals can then react with NO_2 to form peroxynitrates (reaction 4 in Fig. 9) of molecular weight MW $= 344$ g mol^{-1} (identified at m/z 345 in H_3O^+ mode and m/z 344 in NO^+ mode). As with terpinolene, these compounds have not been

detected in the gas or particle phase, suggesting that the pathway is minor. RO_2 radicals can also undergo self-reactions, leading to the formation of a characteristic hydroxynitrate and a ketonitrate (reaction 5 in Fig. 9) of molecular weights $MW = 283$ and $MW = 281\,g\,mol^{-1}$ respectively. The hydroxynitrate has been detected at m/z 284 in H_3O^+ ionization mode and m/z 282 in NO^+ mode and the ketonitrate at m/z 282 ($M + 1$, H_3O^+) and m/z 311 ($M + 30$, NO^+). As mentioned previously, this reaction is only possible when the carbon atom which carries the peroxy group is linked to an H atom so, here, only for one of the two peroxy radicals. Finally, RO_2 radicals can react with another peroxy radical or with NO_3 (reactions 6 and 6′ in Fig. 9) to form an alkoxy radical. This last one can react with O_2 to form a ketonitrate ($MW = 281\,g\,mol^{-1}$). The alkoxy radicals can decompose by a scission of the $C(ONO_2)$–$CH(O^{\bullet})$ bond associated with a loss of NO_2 to form a dicarbonyl product of $MW = 236\,g\,mol^{-1}$ (m/z 237 in H_3O^+ mode and m/z 236 in NO^+ mode, reaction 9, framed in orange in Fig. 9). It can also decompose by a C–C breaking on the other side of the alkoxy group (reaction 8 in Fig. 9) to form a trifunctional compound ($MW = 298\,g\,mol^{-1}$), detected at m/z 299 (H_3O^+) and m/z 298 (NO^+). It should be noted that, in the case where the NO_3 radical adds on to the exocyclic double bond, formaldehyde is expected to be formed (see Fig. S3), but it was not detected with FTIR (with a detection limit close to 10 ppb). This information confirms that this pathway is minor.

Even though the reaction of NO_3 on the remaining $CH_2{=}C{<}$ double bond is expected to be slow, secondary products have been detected and shown in red in Fig. 9. Second-generation epoxides ($MW = 252\,g\,mol^{-1}$, m/z 253 in H_3O^+ mode and m/z 252 in NO^+ mode; $MW = 222\,g\,mol^{-1}$, m/z 223 in H_3O^+ mode and m/z 222 in NO^+ mode) have been measured (reaction 3 in Fig. 9). Also a carbonyl compound of $MW = 238\,g\,mol^{-1}$ (m/z 239 in H_3O^+ mode and m/z 238 in NO^+ mode) coming from the decomposition of the alkoxy radical (reaction 8-2) has been detected. A trifunctional species can also be formed by the reaction of the alkoxy radicals with O_2 (reaction 8-2 in Fig. 9). This diketonitrate ($MW = 313\,g\,mol^{-1}$) was detected in H_3O^+ mode (m/z 314). Finally, a nitrogen product which can be a dinitrate has been detected at m/z 327 in NO^+ ionization mode but has not been identified.

As with terpinolene, estimated vapor pressures of detected products and the corresponding partitioning ratio between the gas and aerosol phase are shown next to the products in Fig. 9. Because β-caryophyllene is a sesquiterpene (C_{15}), most of the oxidation products have very low vapor pressures and can thus contribute to SOA formation. This is in good agreement with the high SOA yields observed even for low aerosol mass loading. Only a few products formed by fragmentation processes have relatively high volatility, thus explaining SOA yields between 50 % and 90 % and not 100 %.

Finally, many identified products are also organic nitrates, in good agreement with gas-phase observations.

The study of Wu et al. (2021) carried out an identification of SOA composition. Particle-phase molecular composition was identified using both a Filter Inlet for Gases and AEROsols (FIGAERO) coupled with a chemical ionization mass spectrometer (CIMS) and an extractive electrospray ionization time-of-flight mass spectrometer (EESI-ToF). A large majority of organic nitrates were detected. C_{15} monomers are major products, as also shown in our study. C_{30} dimers have also been detected, but they are heavy products and out of the PTR-ToF-MS mass-to-charge ratio range used in our study. In addition, the quantity of dimers detected in the particle phase can be explained by the reaction of hydroxynitrates with carbonyl compounds, via an acid-catalyzed particle-phase reaction leading to the formation of acetal dimers and trimers, as shown in Claflin and Ziemann (2018).
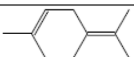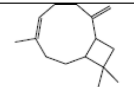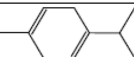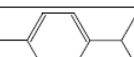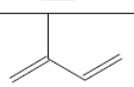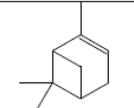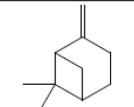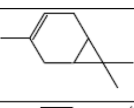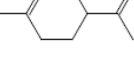
This study is in good agreement with the determination of organic nitrates in the particle phase: a large quantity of organic nitrates was detected, which confirms their prominence in β-caryophyllene $+\,NO_3$ SOA formation. Most of the products were too heavy to be detected in our study, but two major ones are $C_{15}H_{24}O_2$ ($MW = 236\,g\,mol^{-1}$) and $C_{15}H_{25}NO_5$ ($MW = 298\,g\,mol^{-1}$). They have been identified here as opening-ring products. This confirms the importance of these two products in β-caryophyllene $+\,NO_3$ chemistry.

5   Discussion and comparison

Yields measured in this study are summarized in Table 5 and compared to those obtained for other BVOCs by previous studies. It can be observed that oxidation of terpinolene and β-caryophyllene produces large amounts of SOA and ONs, similarly to other BVOCs, with two notable exceptions for α-pinene and α-terpinene. In the case of α-pinene, larger formation yield of carbonyls was observed in comparison to the others BVOCs (Ng et al., 2017). These carbonyl compounds being more volatile than ONs, several previous studies suggest that there is a correlation between ONs and SOA yields (Hallquist et al., 1999; Fry et al., 2014). Indeed, α-pinene has a low organic nitrate yield, corresponding to almost no SOA production, when limonene and Δ-carene both exhibit high SOA and organic nitrate yields. However, the results obtained in a previous comparative study (Fouqueau et al., 2020b) for α- and γ-terpinene show that α-terpinene does not follow this correlation, as it produces a large quantity of organic nitrates but almost no SOAs. To interpret these observations, the mechanisms have to be considered.

As discussed previously in Sect. 4.3 and also in Fouqueau et al. (2020a), two mechanism steps are critical for SOA formation: the peroxy and the alkoxy reaction pathways. For the peroxy radicals, this study has shown the hydroxynitrates coming from the reaction $RO_2 + RO_2 \rightarrow ROH + R(O)$ have

Table 5. Mean SOA and organic nitrate yields obtained in this study for terpinolene and β-caryophyllene and for other terpenes in the literature.

Compound	Formula	Y_{SOA} (10 µg m^{-3})	$Y_{ON, total}$	$Y_{ONp, mass}$ / $Y_{SOA, mass}$	Ref.
Terpinolene		5 %	69 % ± 24 %	28 % – 66 %	This study
β-Caryophyllene		40 %	79 % ± 23 %	79 %	This study
γ-Terpinene		10 %	55 % ± 15 %	7 % – 50 %	Fouqueau et al. (2020a)
α-Terpinene		1.2 %	48 % ± 12 %	86 % – 125 %	Fouqueau et al. (2020a)
Isoprene		12 %	62 % – 78 %	/	Ng et al. (2008), Rollins et al. (2009)
α-Pinene		0 %	10 %	/	Fry et al. (2014)
β-Pinene		33 % – 44 %	45 % – 74 %	/	Boyd et al. (2015), Fry et al. (2014)
Δ-Carene		38 % – 65 %	77 %	/	Fry et al. (2014)
Limonene		44 % – 57 %	77 %	/	Fry et al. (2014)

low vapor pressures and can contribute to SOA formation. In the case of terpinolene, this reaction is less favorable than for β-terpinene, for example, because the reaction is estimated to proceed mainly by addition of NO$_3$ onto the fully substituted exocyclic double bond, leading to tertiary peroxy radicals. Even though these hydroxynitrates were detected, their formation yields should be low. For the alkoxy radicals, several decomposition pathways can occur, forming different types of products having different volatilities: the scission of the C(ONO$_2$)–CH(O$^\bullet$) bond leads to the formation of volatile dicarbonyl products. On the contrary, when the alkoxy decomposes by a scission of the C–C bond located on the other side of the alkoxy group, it produces a keto-nitrooxy-alkyl radical which then evolves to form a low-vapor trifunctional species (diketonitrate). The major role of these two steps has already been pointed out by previous studies. The role of the RO$_2$ + RO$_2$ reaction has been shown to play a significant role in SOA formation from isoprene (Ng et al., 2008). The role of the alkoxy radical decomposition has already been raised by Kurten et al. (2017), suggesting that for Δ-carene, which has a high SOA yield, the decomposition of alkoxy radicals can lead to the formation of keto-nitrooxy-alkyl radicals, whereas

for α-pinene, the alkoxy radicals decompose almost exclusively to form the dicarbonyl compound, explaining the low SOA and ON yields. The mechanisms of terpinolene are thus in good agreement with these previous studies.

SOA yields obtained for β-caryophyllene are very high, and this can easily be explained by the size of this precursor (C$_{15}$). β-Caryophyllene is the only sesquiterpene for which data have been provided, and comparison of its SOA yield with those obtained for terpenes is not fully relevant. Nevertheless, the same key steps have been noted in the mechanism. The addition of NO$_3$ onto the endocyclic double bond is expected to be the major pathway leading to the formation of the same types of functionalized products as those observed for terpinolene (hydroxynitrates, ketonitrates, diketonitrates) but here having much lower vapor pressures.

Organic nitrate yields of both studied compounds are around 50 %. They can be compared to those measured for other BVOCs, presented in Table 5: within the uncertainties, they appear to be similar to those of α- and γ-terpinene (48 % and 55 % respectively; Fouqueau et al., 2020a). Limonene has a yield between 30 % and 72 % (Hallquist et al., 1999; Spittler et al., 2006) and β-pinene between

22 % and 74 % (Boyd et al., 2015; Fry et al., 2014; Hallquist et al., 1999). They also appear similar to those of Δ-carene (68 %–77 %; Fry et al., 2014; Hallquist et al., 1999) and isoprene (62 %–78 %; Rollins et al., 2009) within the uncertainties. BVOC + NO$_3$ reactions are therefore major sources of ONs.

Products coming from isomerization were not detected in this study. Even though this is considered a minor pathway by the calculation of Vereecken and Peeters (2009), it was proved to be possible in Aschmann et al. (2012) for cycloalkoxy radicals. Isomerization could thus occur for β-caryophyllene. Products coming from this pathway were searched for, but none was found. Nevertheless, this reaction leads to the formation of heavy functionalized products that can be difficult to measure with a PTR-MS for two reasons: (i) it cannot measure products that are too heavy, which is probably the case for isomerization products of β-caryophyllene, and (ii) these compounds can be found largely in the particle phase. No analysis at the molecular scale was conducted in the particle phase during our experiments. Indeed, in this study we only measure the total organic nitrates in the aerosol phase from their IR absorption band. Nitrates formed by this pathway will not be differenced from other ones. The occurrence of this pathway is thus not in disagreement with the observation of high SOA formation.

For both compounds, epoxides have been detected. They were not quantified, but based on previous studies, their formation yields are expected to be low. Their formation is considered favored only at low oxygen concentration (Berndt and Böge, 1995). Even though their detection has been rare in previous studies, their formation was already observed in the same experimental conditions in Fouqueau et al. (2020a). They were also measured by Skov et al. (1994), who studied the oxidation of some alkenes and isoprene by NO$_3$. Low epoxide yields have also been reported by Wangberg et al. (1997) (3 % for α-pinene) and Ng et al. (2008) (>1 % for isoprene).

6 Conclusions and atmospheric impacts

In summary, this study has provided kinetic and mechanistic data on the reaction between nitrate radicals and two BVOCs, terpinolene and β-caryophyllene. For the first time, an absolute rate determination was conducted for β-caryophyllene. Both compounds have been studied using relative and absolute rate determinations, leading to kinetic data in good agreement. Due to the presence of two double bonds, they appear to be very reactive towards nitrate radicals. As far as we know, this is also the first mechanistic study of the terpinolene + NO$_3$ reaction and the first determination of ON yields for β-caryophyllene. They both produce large amounts of ONs in the gas phase, with yields around 50 %. These compounds have also been detected in the particle phase, with a production yield of 25 % for the two compounds. In

Table 6. Atmospheric lifetimes of terpinolene and β-caryophyllene with respect to their oxidation by NO$_3$ and OH radicals and by ozone.

Compound	τ_{NO_3}*	τ_{NO_3}**	τ_{OH}***	τ_{O_3}***
		(min)		
Terpinolene	1.1	112	38[b]	15[a]
β-Caryophyllene	3.8	381	42[c]	2[a]

* Calculated with [NO$_3$] = 2.5 × 10^8 molecules cm^{-3} (10 ppt).
** Calculated with [NO$_3$] = 2.5 × 10^6 molecules cm^{-3} (0.1 ppt).
*** Calculated with [OH] = 2 × 10^6 molecules cm^{-3} and [O$_3$] = 7 × 10^{11} molecules cm^{-3}.
[a] Calculated with rate constant recommended by IUPAC.
[b] Calculated with rate constant from Corchnoy and Atkinson (1990).
[c] Calculated with rate constant from Shu and Atkinson (1995).

total, these reactions produce around 70 %–80 % of organic nitrates. These compounds were also shown to be good SOA precursors. At 10 µg m^{-3}, terpinolene has an SOA yield of 5 % when β-caryophyllene has a yield of 40 %. The latter produces a high amount of SOA, even for low aerosol mass loading. For both compounds, SOA formation has been explained thanks to the detection of oxidation products at the molecular scale, which allowed proposing mechanisms. The SOA yield of terpinolene can be explained by the formation of two types of low-volatility product: a trifunctional species and a hydroxynitrate. High SOA yields observed for β-caryophyllene can be explained by the formation of several high-molecular-weight products. For both compounds, preferential pathways have been proposed.

In order to evaluate the contribution of the NO$_3$-initiated oxidation to the total degradation of these BVOCs, atmospheric lifetimes have been estimated using NO$_3$ concentrations of 10 ppt (typical nighttime concentration) and 0.1 ppt (low-insolation diurnal concentration; Khan et al., 2015). It should be noted that terpinolene is intensively emitted during both the day and the night (Lindwall et al., 2015). These lifetimes are compared to those estimated for OH and ozone oxidation in Table 6. It can be observed that terpinolene and β-caryophyllene have very short lifetimes (a few minutes) towards the NO$_3$ radical in nighttime conditions, confirming that NO$_3$ oxidation is a major sink for these compounds. During the day, in low-sunlight conditions, lifetimes are still short (between 2 and 7 h). They nevertheless are longer than those estimated for OH and ozone chemistries. NO$_3$ is thus a minor oxidant under these diurnal conditions. These short lifetimes also demonstrate that oxidation products will be formed close to the emission area.

One characteristic feature of the oxidation of BVOCs by the NO$_3$ radical is that it produces large amounts of organic nitrates in both gas and aerosol phases. Even though OH-initiated oxidation can also produce organic nitrates (through RO$_2$ + NO reactions), yields are usually lower (Lee et al., 2006). Another major finding of this study is that the NO$_3$ ox-

idation of β-caryophyllene and to a lesser extent of terpinolene produces large amounts of SOA. The yields obtained in this study can be compared to those measured in previous studies for ozonolysis and OH oxidation. First, concerning the oxidation by OH radicals, SOA yields measured for terpinolene were shown to be close to those measured for NO_3 oxidation: for low-NO_x conditions, the SOA yield was found to be around 3 % at $M_0 = 10\,\mu g\,m^{-3}$, but that can reach 40 % for higher aerosol mass loadings (Friedman and Farmer, 2018; Lee et al., 2006b). For β-caryophyllene, the SOA yields were shown to reach 68 % (Lee et al., 2006b). Regarding the ozonolysis, SOA yields have been found to be 20 % for terpinolene and 45 % for β-caryophyllene (Lee et al., 2006a). Regarding these results, the oxidation by NO_3 produces similar amounts of SOA to the other oxidants. However, the chemical composition of the aerosol phase is significantly different.

In conclusion, the most important impacts of this chemistry rely on the formation of large amounts of organic nitrates (present in both gas and aerosol phases) and SOA. Organic nitrates play a key role in tropospheric chemistry because they behave as NO_x reservoirs, carrying reactive nitrogen in remote areas. Their chemistry in gas and aerosol phases is nevertheless still not well documented. Considering that our study shows large production of multifunctional organic nitrates, it is necessary to better understand their reactivity in order to better evaluate their impacts. Formation of SOA seems, on the other hand, to be strongly dependent on the structure of the BVOC. Studies at a molecular scale are thus crucial to better evaluate the impact of this chemistry on SOA formation.

Author contributions. BPV and MCi coordinated the research project. AF, BPV, MCi and JFD designed the experiments in the simulation chambers. AF performed the experiments with the technical support of MCa and EP and performed the data treatment and interpretation with MCi and BPV. AF, BPV and MCi wrote the pa-per, and AF was responsible for the final version of the paper. All co-authors revised the content of the original manuscript and approved the final version of the paper.

References

Aoki, N., Inomata, S., and Tanimoto, H.: Detection of C_1-C_5 alkyl nitrates by proton transfer reaction time-of-flight mass spectrometry, Int. J. Mass. Spectrom., 263, 12–21, 2007.

Aschmann, S. M., Arey, J., and Atkinson, R.: Kinetics and Products of the Reactions of OH Radicals with Cyclohexene, 1-Methyl-1-cyclohexene, cis-Cyclooctene, and cis-Cyclodecene, J. Phys. Chem. A., 116, 9507–15, https://doi.org/10.1021/jp307217m, 2012.

Atkinson, R.: Kinetics and mechanisms of the gas-phase reactions of the hydroxyl radical with organic compounds under atmospheric conditions, Chem. Rev., 86, 69–201, 1986.

Atkinson, R., Plum, C. N., Carter, W. P. L., Winer, A. M., and Pitts, J. N.: Rate constants for the gas-phase reactions of nitrate radicals with a series of organics in air at $298.+-.1\,K$, J. Phys. Chem., 88, 1210–1215, https://doi.org/10.1021/j150650a039, 1984a.

Atkinson, R., Aschmann, S. M., Winer, A. M., and Pitts, J. N.: Kinetics of the gas-phase reactions of nitrate radicals with a series of dialkenes, cycloalkenes, and monoter-

penes at 295 .+−. 1 K, Environ. Sci. Technol., 18, 370–375, https://doi.org/10.1021/es00123a016, 1984b.

Atkinson, R., Aschmann, S. M., and Pitts, J. N.: Rate constants for the gas-phase reactions of the nitrate radical with a series of organic compounds at 296 .+−. 2 K, 92, 3454–3457, https://doi.org/10.1021/j100323a028, 1988.

Benter, T., Becker, E., Wille, U., Rahman, M. M., and Schindler, R. N.: The Determination of Rate Constants for the Reactions of Some Alkenes with the NO$_3$ Radical, Berichte der Bunsengesellschaft für physikalische Chemie, 96, 769–775, https://doi.org/10.1002/bbpc.19920960607, 1992.

Berndt, T. and Böge, O.: Products and Mechanism of the Reaction of NO$_3$ with Selected Acyclic Monoalkenes, J. Atmos. Chem., 21, 275–291, 1995.

Berndt, T., Kind, I., and Karbach, H.-J.: Kinetics of the Gas-Phase Reaction of NO$_3$ Radicals with 1-Butene, trans-Butene, 2-Methyl-2-butene and 2,3-Dimethyl-2-butene Using LIF Detection, Berichte der Bunsengesellschaft für physikalische Chemie, 102, 1486–1491, https://doi.org/10.1002/bbpc.199800017, 1998.

Boyd, C. M., Sanchez, J., Xu, L., Eugene, A. J., Nah, T., Tuet, W. Y., Guzman, M. I., and Ng, N. L.: Secondary organic aerosol formation from the β-pinene+NO$_3$ system: effect of humidity and peroxy radical fate, Atmos. Chem. Phys., 15, 7497–7522, https://doi.org/10.5194/acp-15-7497-2015, 2015.

Brown, S. S. and Stutz, J.: Nighttime radical observations and chemistry, Chem. Soc. Rev., 41, 6405–6447, https://doi.org/10.1039/C2CS35181A, 2012.

Calvert, J. G., Orlando, J. J., Stockwell, W. R., and Wallington, T. J.: The Mechanisms of Reactions Influencing Atmospheric Ozone, Oxford University Press, New York, ISBN: 9780190233020, 2015.

Claflin, M. S. and Ziemann, P. J.: Identification and Quantitation of Aerosol Products of the Reaction of β-Pinene with NO$_3$ Radicals and Implications for Gas- and Particle-Phase Reaction Mechanisms, J. Phys. Chem. A, 122, 3640–3652, https://doi.org/10.1021/acs.jpca.8b00692, 2018.

Corchnoy, S. B. and Atkinson, R.: Kinetics of the gas-phase reactions of hydroxyl and nitrogen oxide (NO$_3$) radicals with 2-carene, 1,8-cineole, p-cymene, and terpinolene, Environ. Sci. Technol., 24, 1497–1502, 1990.

Doussin, J.-F., Durand-Jolibois, R., Ritz, D., Monod, A., and Carlier, P.: Design of an environmental chamber for the study of atmospheric chemistry: New developments in the analytical device, 25, 236 p., 1997.

Draper, D. C., Farmer, D. K., Desyaterik, Y., and Fry, J. L.: A qualitative comparison of secondary organic aerosol yields and composition from ozonolysis of monoterpenes at varying concentrations of NO$_2$, Atmos. Chem. Phys., 15, 12267–12281, https://doi.org/10.5194/acp-15-12267-2015, 2015.

Duncianu, M., David, M., Kartigueyane, S., Cirtog, M., Doussin, J.-F., and Picquet-Varrault, B.: Measurement of alkyl and multifunctional organic nitrates by proton-transfer-reaction mass spectrometry, Atmos. Meas. Tech., 10, 1445–1463, https://doi.org/10.5194/amt-10-1445-2017, 2017.

Fouqueau, A., Cirtog, M., Cazaunau, M., Pangui, E., Doussin, J.-F., and Picquet-Varrault, B.: A comparative and experimental study of the reactivity with nitrate radical of two terpenes: α-terpinene and γ-terpinene, Atmos. Chem. Phys., 20, 15167–15189, https://doi.org/10.5194/acp-20-15167-2020, 2020a.

Fouqueau, A., Cirtog, M., Cazaunau, M., Pangui, E., Zapf, P., Siour, G., Landsheere, X., Méjean, G., Romanini, D., and Picquet-Varrault, B.: Implementation of an incoherent broadband cavity-enhanced absorption spectroscopy technique in an atmospheric simulation chamber for in situ NO$_3$ monitoring: characterization and validation for kinetic studies, Atmos. Meas. Tech., 13, 6311–6323, https://doi.org/10.5194/amt-13-6311-2020, 2020b.

Fouqueau, A., Cirtog, M., Cazaunau, M., Pangui, E., Doussin, J.-F., and Picquet-Varrault, B.: Library of Advanced Data Products: Photolysis Frequencies & Quantum yields [data set], https://data.eurochamp.org/data-access/photolysis-frequencies-quantum-yields/ (last access: 1 May 2021), 2021a.

Fouqueau, A., Cirtog, M., Cazaunau, M., Pangui, E., Doussin, J.-F., and Picquet-Varrault, B.: Database of Atmospheric Simulation Chamber Studies [data set], https://data.eurochamp.org/data-access/chamber-experiments/ (last access: 1 May 2021), 2021b.

Friedman, B. and Farmer, D. K.: SOA and gas phase organic acid yields from the sequential photooxidation ofseven monoterpenes, Atmos. Environ., 187, 335–345, 2018.

Fry, J. L., Draper, D. C., Barsanti, K. C., Smith, J. N., Ortega, J., Winkler, P. M., Lawler, M. J., Brown, S. S., Edwards, P. M., Cohen, R. C., and Lee, L.: Secondary Organic Aerosol Formation and Organic Nitrate Yield from NO$_3$ Oxidation of Biogenic Hydrocarbons, Environ. Sci. Technol., 48, 11944–11953, https://doi.org/10.1021/es502204x, 2014.

Geron, C., Rasmussen, R., R. Arnts, R., and Guenther, A.: A review and synthesis of monoterpene speciation from forests in the United States, Atmos. Environ., 34, 1761–1781, https://doi.org/10.1016/S1352-2310(99)00364-7, 2000.

Gómez-González, Y., Surratt, J. D., Cuyckens, F., Szmigielski, R., Vermeylen, R., Jaoui, M., Lewandowski, M., Offenberg, J. H., Kleindienst, T. E., Edney, E. O., Blockhuys, F., Alsenoy, C. V., Maenhaut, W., and Claeys, M.: Characterization of organosulfates from the photooxidation of isoprene and unsaturated fatty acids in ambient aerosol using liquid chromatography/(-) electrospray ionization mass spectrometry, J. Mass. Spectrom., 43, 371–382, 2008.

Gordon, I. E., Rothman, L. S., Hill, C., Kochanov, R. V., Tan, Y., Bernath, P. F., Birk, M., Boudon, V., Campargue, A., Chance, K. V., Drouin, B. J., Flaud, J.-M., Gamache, R. R., Hodges, J. T., Jacquemart, D., Perevalov, V. I., Perrin, A., Shine, K. P., Smith, M.-A. H., Tennyson, J., Toon, G. C., Tran, H., Tyuterev, V. G., Barbe, A., Császár, A. G., Devi, V. M., Furtenbacher, T., Harrison, J. J., Hartmann, J.-M., Jolly, A., Johnson, T. J., Karman, T., Kleiner, I., Kyuberis, A. A., Loos, J., Lyulin, O. M., Massie, S. T., Mikhailenko, S. N., Moazzen-Ahmadi, N., Müller, H. S. P., Naumenko, O. V., Nikitin, A. V., Polyansky, O. L., Rey, M., Rotger, M., Sharpe, S. W., Sung, K., Starikova, E., Tashkun, S. A., Auwera, J. V., Wagner, G., Wilzewski, J., Wcisło, P., Yu, S., and Zak, E. J.: The HITRAN2016 molecular spectroscopic database, J. Quant. Spectrosc. Ra., 203, 3–69, https://doi.org/10.1016/j.jqsrt.2017.06.038, 2017.

Guenther, A., Hewitt, C. N., Erickson, D., Fall, R., Geron, C., Graedel, T., Harley, P., Klinger, L., Lerdau, M., Mckay, W. A., Pierce, T., Scholes, B., Steinbrecher, R., Tallamraju, R., Taylor, J., and Zimmerman, P.: A global model of natural volatile organic

compound emissions, J. Geophys. Res.-Atmos., 100, 8873–8892, 1995.

Guenther, A. B., Jiang, X., Heald, C. L., Sakulyanontvittaya, T., Duhl, T., Emmons, L. K., and Wang, X.: The Model of Emissions of Gases and Aerosols from Nature version 2.1 (MEGAN2.1): an extended and updated framework for modeling biogenic emissions, Geosci. Model Dev., 5, 1471–1492, https://doi.org/10.5194/gmd-5-1471-2012, 2012.

Hallquist, M., Wangberg, I., Ljungstrom, E., Barnes, I., and Becker, E.: Aerosol and Product Yields from NO_3 Radical-Initiated Oxidation of Selected Monoterpenes, Environ. Sci. Technol., 33, 553–559, 1999.

Hao, L. Q., Kortelainen, A., Romakkaniemi, S., Portin, H., Jaatinen, A., Leskinen, A., Komppula, M., Miettinen, P., Sueper, D., Pajunoja, A., Smith, J. N., Lehtinen, K. E. J., Worsnop, D. R., Laaksonen, A., and Virtanen, A.: Atmospheric submicron aerosol composition and particulate organic nitrate formation in a boreal forestland–urban mixed region, Atmos. Chem. Phys., 14, 13483–13495, https://doi.org/10.5194/acp-14-13483-2014, 2014.

Hjorth, J., Ottobrini, G., Cappellani, F., and Restelli, G.: A Fourier transform infrared study of the rate constant of the homogeneous gas-phase reaction nitrogen oxide (N_2O_5)+ water and determination of absolute infrared band intensities of N_2O_5 and nitric acid, J. Phys. Chem., 91, 1565–1568, https://doi.org/10.1021/j100290a055, 1987.

Iinuma, Y., Müller, C., Berndt, T., Böge, O., Claeys, M., and Herrmann, H.: Evidence for the Existence of Organosulfates from β-Pinene Ozonolysis in Ambient Secondary Organic Aerosol, Environ. Sci. Technol., 41, 6678–6683, https://doi.org/10.1021/es070938t, 2007.

Ito, A., Sillman, S., and Penner, J. E.: Effects of additional non-methane volatile organic compounds, organic nitrates, and direct emissions of oxygenated organic species on global tropospheric chemistry, J. Geophys. Res.-Atmos., 112, D06309, https://doi.org/10.1029/2005JD006556, 2007.

Jaoui, M., Kleindienst, T. E., Docherty, K. S., Lewandowski, M., and Offenberg, J. H.: Secondary organic aerosol formation from the oxidation of a series of sesquiterpenes: α-cedrene, β-caryophyllene, α-humulene and α-farnesene with O_3, OH and NO_3 radicals, Environ. Chem., 10, 178–193, 2013.

Kerdouci, J., Picquet-Varrault, B., and Doussin, J. F.: Structure–activity relationship for the gas-phase reactions of NO_3 radical with organic compounds: Update and extension to aldehydes, Atmos. Environ., 84, 363–372, https://doi.org/10.1016/j.atmosenv.2013.11.024, 2014.

Khan, M. A. H., Morris, W. C., Watson, L. A., Galloway, M., Hamer, P. D., Shallcross, B. M. A., Percival, C. J., and Shallcross, D. E.: Estimation of Daytime NO_3 Radical Levels in the UK Urban Atmosphere Using the Steady State Approximation Method, Adv. Meteorol., 2015, e294069, https://doi.org/10.1155/2015/294069, 2015.

Kiendler-Scharr, A., Mensah, A., Friese, E., Topping, D., Nemitz, E., Prevot, A. S. H., Äijälä, M., Allan, J., Canonaco, F., Canagaratna, M., Carbone, S., Crippa, M., Dall'Osto, M., Day, D. A., De Carlo, P., Di Marco, C. F., Elbern, H., Eriksson, A., Freney, E., Hao, L., Herrmann, H., Hildebrandt, L., Hillamo, R., Jimenez, J. L., Laaksonen, A., McFiggans, G., Mohr, C., O'Dowd, C., Otjes, R., Ovadnevaite, J., Pandis, S. N., Poulain, L., Schlag, P., Sellegri, K., Swietlicki, E., Tiitta, P., Ver-

meulen, A., Wahner, A., Wornsnop, D., and Wu, H.-C.: Ubiquity of organic nitrates from nighttime chemistry in the European submicron aerosol, Geophys. Res. Lett., 43, 7735–7744, https://doi.org/10.1002/2016GL069239, 2016.

Kurten, T., Moller, K. H., Nguyen, T. B., Schwantes, R. H., Misztal, P. K., Su, L., Wennberg, P. O., Fry, J. L., and Kjaergaard, H. G.: Alkoxy Radical Bond Scissions Explain the Anomalously Low Secondary Organic Aerosol and Organonitrate Yields From α-Pinene + NO_3, J. Phys. Chem. Lett., 8, 2826–2834, https://doi.org/10.1021/acs.jpclett.7b01038, 2017.

Lai, A. C. K. and Nazaroff, W. W.: Modeling indoor particle deposition from turbulent flow onto smooth surfaces, J. Aerosol Sci., 31, 463–476, https://doi.org/10.1016/S0021-8502(99)00536-4, 2000.

Lamkaddam, H., Gratien, A., Pangui, E., Cazaunau, M., Picquet-Varrault, B., and Doussin, J.-F.: High-NO_x Photooxidation of n-Dodecane: Temperature Dependence of SOA Formation, Environ. Sci. Technol., 51, 192–201, https://doi.org/10.1021/acs.est.6b03821, 2017.

Lancar, I. T., Daele, V., Lebras, G., and Poulet, G.: Reaction of NO_3 radicals with 2,3-dimethylbut-2-ene, buta-1,3-diene and 2,3-dimethylbuta-1,3-diene, J. Chim. Phys. Pcb., 88, 1777–1792, 1991.

Lee, A., Goldstein, A. H., Kroll, J. H., Ng, N. L., Varutbangkul, V., Flagan, R. C., and Seinfeld, J. H.: Gas-phase products and secondary aerosol yields from the photooxidation of 16 different terpenes, 111, D17305, https://doi.org/10.1029/2006JD007050, 2006.

Lee, B. H., Mohr, C., Lopez-Hilfiker, F. D., Lutz, A., Hallquist, M., Lee, L., Romer, P., Cohen, R. C., Iyer, S., Kurten, T., Hu, W., Day, D. A., Campuzano-Jost, P., Jimenez, J. L., Xu, L., Ng, N. L., Guo, H., Weber, R. J., Wild, R. J., Brown, S. S., Koss, A., de Gouw, J. A., Olson, K., Goldstein, A. H., Seco, R., Kim, S., McAvey, K., Shepson, P. B., Starn, T., Baumann, K., Edgerton, E. S., Liu, J., Shilling, J. E., Miller, D. O., Brune, W., Schobesberger, S., D'Ambro, E. L., and Thornton, J. A.: Highly functionalized organic nitrates in the southeast United States: Contribution to secondary organic aerosol and reactive nitrogen budgets, P. Natl. Acad. Sci. USA, 113, 1516–1521, https://doi.org/10.1073/pnas.1508108113, 2016.

Lindwall, F., Faubert, P., and Rinnan, R.: Diel Variation of Biogenic Volatile Organic Compound Emissions–A field Study in the Sub, Low and High Arctic on the Effect of Temperature and Light, PLoS ONE, 10, e0123610, https://doi.org/10.1371/journal.pone.0123610, 2015.

Martinez, E., Cabanas, B., Aranda, A., Martin, P., Notario, A., and Salgado, S.: Study on the NO_3 Radical Reactivity: Reactions with Cyclic Alkenes, J. Phys. Chem. A, 103, 5321–5327, 1999.

McGillen, M. R., Carter, W. P. L., Mellouki, A., Orlando, J. J., Picquet-Varrault, B., and Wallington, T. J.: Database for the kinetics of the gas-phase atmospheric reactions of organic compounds, Earth Syst. Sci. Data, 12, 1203–1216, https://doi.org/10.5194/essd-12-1203-2020, 2020.

Müller, M., Graus, M., Wisthaler, A., Hansel, A., Metzger, A., Dommen, J., and Baltensperger, U.: Analysis of high mass resolution PTR-TOF mass spectra from 1,3,5-trimethylbenzene (TMB) environmental chamber experiments, Atmos. Chem. Phys., 12, 829–843, https://doi.org/10.5194/acp-12-829-2012, 2012.

Newland, M. J., Ren, Y., McGillen, M. R., Michelat, L., Daële, V., and Mellouki, A.: NO$_3$ chemistry of wildfire emissions: a kinetic study of the gas-phase reactions of furans with the NO$_3$ radical, Atmos. Chem. Phys., 22, 1761–1772, https://doi.org/10.5194/acp-22-1761-2022, 2022.

Ng, N. L., Kwan, A. J., Suratt, J. D., Chan, A. W. H., Chhabra, P. S., Sorooshian, A., Pye, H. O. T., Crounse, J. D., Wennberg, P. O., Flagan, R. C., and Seinfeld, J. H.: Secondary organic aerosol (SOA) formation from reaction of isoprene with nitrate radicals (NO$_3$), 8, 4117–4140, 2008.

Ng, N. L., Brown, S. S., Archibald, A. T., Atlas, E., Cohen, R. C., Crowley, J. N., Day, D. A., Donahue, N. M., Fry, J. L., Fuchs, H., Griffin, R. J., Guzman, M. I., Herrmann, H., Hodzic, A., Iinuma, Y., Jimenez, J. L., Kiendler-Scharr, A., Lee, B. H., Luecken, D. J., Mao, J., McLaren, R., Mutzel, A., Osthoff, H. D., Ouyang, B., Picquet-Varrault, B., Platt, U., Pye, H. O. T., Rudich, Y., Schwantes, R. H., Shiraiwa, M., Stutz, J., Thornton, J. A., Tilgner, A., Williams, B. J., and Zaveri, R. A.: Nitrate radicals and biogenic volatile organic compounds: oxidation, mechanisms, and organic aerosol, Atmos. Chem. Phys., 17, 2103–2162, https://doi.org/10.5194/acp-17-2103-2017, 2017.

Odum, J. R., Hoffmann, T., Bowman, F., Collins, D., Flagan, R. C., and Seinfeld, J. H.: Gas/Particle Partitioning and Secondary Organic Aerosol Yields, Environ. Sci. Technol., 30, 2580–2585, 1996.

Orphal, J., Fellows, C. E., and Flaud, P.-M.: The visible absorption spectrum of NO$_3$ measured by high-resolution Fourier transform spectroscopy, 108, 4077, https://doi.org/10.1029/2002JD002489, 2003.

Pankow, J. F. and Asher, W. E.: SIMPOL.1: a simple group contribution method for predicting vapor pressures and enthalpies of vaporization of multifunctional organic compounds, Atmos. Chem. Phys., 8, 2773–2796, https://doi.org/10.5194/acp-8-2773-2008, 2008.

Picquet-Varrault, B., Scarfogliero, M., Ait Helal, W., and Doussin, J.-F.: Reevaluation of the rate constant for the reaction propene +NO$_3$ by absolute rate determination, International Journal of Chemical Kinetics, 41, 73–81, 2009.

Picquet-Varrault, B., Suarez-Bertoa, R., Duncianu, M., Cazaunau, M., Pangui, E., David, M., and Doussin, J.-F.: Photolysis and oxidation by OH radicals of two carbonyl nitrates: 4-nitrooxy-2-butanone and 5-nitrooxy-2-pentanone, Atmos. Chem. Phys., 20, 487–498, https://doi.org/10.5194/acp-20-487-2020, 2020.

Rahman, M. M., Becker, E., Benter, Th., and Schindler, R. N.: A Gasphase Kinetic Investigation of the System F +HNO$_3$ and the Determination of Absolute Rate Constants for the Reaction of the NO$_3$ Radical with CH$_3$SH, 2-Methylpropene, 1,3-Butadiene and 2,3-Dimethyl-2-Butene, Berichte der Bunsengesellschaft für physikalische Chemie, 92, 91–100, https://doi.org/10.1002/bbpc.198800018, 1988.

Rindelaub, J. D., McAvey, K. M., and Shepson, P. B.: The photochemical production of organic nitrates from a-pinene and loss via acid-dependent particle phase hydrolysis, Atmos. Environ., 100, 193–201, 2015.

Rollins, A. W., Kiendler-Scharr, A., Fry, J. L., Brauers, T., Brown, S. S., Dorn, H.-P., Dubé, W. P., Fuchs, H., Mensah, A., Mentel, T. F., Rohrer, F., Tillmann, R., Wegener, R., Wooldridge, P. J., and Cohen, R. C.: Isoprene oxidation by nitrate radical: alkyl nitrate and secondary organic aerosol yields, Atmos. Chem. Phys., 9, 6685–6703, https://doi.org/10.5194/acp-9-6685-2009, 2009.

Rothman, L. S., Barbe, A., Chris Benner, D., Brown, L. R., Camy-Peyret, C., Carleer, M. R., Chance, K., Clerbaux, C., Dana, V., Devi, V. M., Fayt, A., Flaud, J.-M., Gamache, R. R., Goldman, A., Jacquemart, D., Jucks, K. W., Lafferty, W. J., Mandin, J.-Y., Massie, S. T., Nemtchinov, V., Newnham, D. A., Perrin, A., Rinsland, C. P., Schroeder, J., Smith, K. M., Smith, M. A. H., Tang, K., Toth, R. A., Vander Auwera, J., Varanasi, P., and Yoshino, K.: The HITRAN molecular spectroscopic database: edition of 2000 including updates through 2001, J. Quant. Spectrosc. Ra., 82, 5–44, https://doi.org/10.1016/S0022-4073(03)00146-8, 2003.

Schott, G. and Davidson, N.: Shock waves in chemical kinetics: The decomposition of N$_2$O$_5$ at high temperatures, 80, 1841–1853, 1958.

Shu, Y. and Atkinson, R.: Atmospheric lifetimes and fates of a series of sesquiterpenes, 100, 7275–7281, 1995.

Skov, H., Benter, T., Schindler, R. N., Hjorth, J., and Restelli, G.: Epoxide formation in the reactions of the nitrate radical with 2,3-dimethyl-2-butene, cis- and trans-2-butene and isoprene, Atmos. Environ., 28, 1583–1592, 1994.

Slade, J. H., de Perre, C., Lee, L., and Shepson, P. B.: Nitrate radical oxidation of γ-terpinene: hydroxy nitrate, total organic nitrate, and secondary organic aerosol yields, Atmos. Chem. Phys., 17, 8635–8650, https://doi.org/10.5194/acp-17-8635-2017, 2017.

Spittler, M., Barnes, I., Bejan, I., Brockmann, K. J., Benter, Th., and Wirtz, K.: Reactions of NO$_3$ radicals with limonene and α-pinene: Product and SOA formation, Atmos. Environ., 40, 116–127, https://doi.org/10.1016/j.atmosenv.2005.09.093, 2006.

Stewart, D. J., Almabrok, S. H., Lockhart, J. P., Mohamed, O. M., Nutt, D. R., Pfrang, C., and Marston, G.: The kinetics of the gas-phase reactions of selected monoterpenes and cyclo-alkenes with ozone and the NO$_3$ radical, Atmos. Environ., 70, 227–235, https://doi.org/10.1016/j.atmosenv.2013.01.036, 2013.

Suarez-Bertoa, R., Picquet-Varrault, B., Tamas, W., Pangui, E., and Doussin, J.-F.: Atmospheric Fate of a Series of Carbonyl Nitrates: Photolysis Frequencies and OH-Oxidation Rate Constants, Environ. Sci. Technol., 46, 12502–12509, 2012.

Valorso, R., Aumont, B., Camredon, M., Raventos-Duran, T., Mouchel-Vallon, C., Ng, N. L., Seinfeld, J. H., Lee-Taylor, J., and Madronich, S.: Explicit modelling of SOA formation from α-pinene photooxidation: sensitivity to vapour pressure estimation, Atmos. Chem. Phys., 11, 6895–6910, https://doi.org/10.5194/acp-11-6895-2011, 2011.

Vandaele, A. C., Hermans, C., Simon, P. C., Carleer, M., Colin, R., Fally, S., Mérienne, M. F., Jenouvrier, A., and Coquart, B.: Measurements of the NO$_2$ absorption cross-section from $42\,000\,\mathrm{cm}^{-1}$ to $10\,000\,\mathrm{cm}^{-1}$ (238–1000 nm) at 220 K and 294 K, J. Quant. Spectrosc. Ra., 59, 171–184, 1997.

Vereecken, L. and Peeters, J.: Decomposition of substituted alkoxy radicals – part I: a generalized structure–activity relationship for reaction barrier heightsw, Phys. Chem. Chem. Phys., 11, 9062–9074, https://doi.org/10.1039/b909712k, 2009.

Wangberg, I., Barnes, I., and Becker, K. H.: Product and mechanistic study of the reaction of NO$_3$ radicals with alpha-pinene, Environ. Sci. Technol., 31, 2130–2135, 1997.

Wang, J., Doussin, J.-F., Perrier, S., Perraudin, E., Katrib, Y., Pangui, E., and Picquet-Varrault, B.: Design of a new multi-phase

experimental simulation chamber for atmospheric photosmog, Aerosol and Cloud Chemistry Research, 4, 2465–2494, 2011.

Wu, C., Bell, D. M., Graham, E. L., Haslett, S., Riipinen, I., Baltensperger, U., Bertrand, A., Giannoukos, S., Schoonbaert, J., El Haddad, I., Prevot, A. S. H., Huang, W., and Mohr, C.: Photolytically induced changes in composition and volatility of biogenic secondary organic aerosol from nitrate radical oxidation during night-to-day transition, Atmos. Chem. Phys., 21, 14907–14925, https://doi.org/10.5194/acp-21-14907-2021, 2021.

Xu, L., Suresh, S., Guo, H., Weber, R. J., and Ng, N. L.: Aerosol characterization over the southeastern United States using high-resolution aerosol mass spectrometry: spatial and seasonal variation of aerosol composition and sources with a focus on organic nitrates, Atmos. Chem. Phys., 15, 7307–7336, https://doi.org/10.5194/acp-15-7307-2015, 2015.